A Specialized Histone H1 Variant Is Required for Adaptive Responses to Complex Abiotic Stress and Related DNA Methylation in Arabidopsis[1][OPEN]

Kinga Rutowicz[2], Marcin Puzio, Joanna Halibart-Puzio, Maciej Lirski, Maciej Kotliński, Magdalena A. Kroteń, Lukasz Knizewski, Bartosz Lange, Anna Muszewska, Katarzyna Śniegowska-Świerk, Janusz Kościelniak, Roksana Iwanicka-Nowicka, Krisztián Buza, Franciszek Janowiak, Katarzyna Żmuda, Indrek Jõesaar, Katarzyna Laskowska-Kaszub[3], Anna Fogtman, Hannes Kollist, Piotr Zielenkiewicz, Jerzy Tiuryn, Paweł Siedlecki, Szymon Swiezewski, Krzysztof Ginalski, Marta Koblowska, Rafał Archacki, Bartek Wilczynski, Marcin Rapacz, and Andrzej Jerzmanowski*

Institute of Biochemistry and Biophysics, Polish Academy of Sciences, 02–106 Warsaw, Poland (K.R., J.H.-P., M.L., M.Kot., A.M., R.I.-N., A.F., P.Z., P.S., S.S., M.Kob., A.J.); Laboratory of Systems Biology, University of Warsaw, 02–106 Warsaw, Poland (M.P., M.Kot., B.L., R.I.-N., K.L.-K., P.S., M.Kob., R.A., A.J.); Institute of Plant Physiology, University of Rzeszów, 36–100 Kolbuszowa, Poland (J.H.-P.); College of Inter-Faculty Individual Studies in Mathematics and Natural Sciences, University of Warsaw, 02–089 Warsaw, Poland (M.A.K.); Laboratory of Bioinformatics and Systems Biology, Center of New Technologies (L.K., A.M., K.G.), and Institute of Informatics (K.B., J.T., B.W.), University of Warsaw, 02–097 Warsaw, Poland; Department of Plant Physiology, University of Agriculture in Cracow, 30–239 Cracow, Poland (K.Ś.-Ś., J.K., K.Ż., M.R.); Institute of Plant Physiology, Polish Academy of Sciences, 30–239 Cracow, Poland (F.J.); and Institute of Technology, University of Tartu, 50411 Tartu, Tartumaa, Estonia (I.J., H.K.)

ORCID IDs: 0000-0002-7111-6452 (K.B.); 0000-0002-1095-8998 (F.J.); 0000-0002-8115-1649 (K.Ż.); 0000-0002-5331-7840 (A.F.); 0000-0003-1071-1159 (M.R.); 0000-0002-4684-4503 (A.J.).

Linker (H1) histones play critical roles in chromatin compaction in higher eukaryotes. They are also the most variable of the histones, with numerous nonallelic variants cooccurring in the same cell. Plants contain a distinct subclass of minor H1 variants that are induced by drought and abscisic acid and have been implicated in mediating adaptive responses to stress. However, how these variants facilitate adaptation remains poorly understood. Here, we show that the single Arabidopsis (*Arabidopsis thaliana*) stress-inducible variant H1.3 occurs in plants in two separate and most likely autonomous pools: a constitutive guard cell-specific pool and a facultative environmentally controlled pool localized in other tissues. Physiological and transcriptomic analyses of *h1.3* null mutants demonstrate that H1.3 is required for both proper stomatal functioning under normal growth conditions and adaptive developmental responses to combined light and water deficiency. Using fluorescence recovery after photobleaching analysis, we show that H1.3 has superfast chromatin dynamics, and in contrast to the main Arabidopsis H1 variants H1.1 and H1.2, it has no stable bound fraction. The results of global occupancy studies demonstrate that, while H1.3 has the same overall binding properties as the main H1 variants, including predominant heterochromatin localization, it differs from them in its preferences for chromatin regions with epigenetic signatures of active and repressed transcription. We also show that H1.3 is required for a substantial part of DNA methylation associated with environmental stress, suggesting that the likely mechanism underlying H1.3 function may be the facilitation of chromatin accessibility by direct competition with the main H1 variants.

Linker (H1) histones are conserved and ubiquitous structural components of eukaryotic chromatin required for the stabilization of higher order chromatin structure and are generally thought to restrict DNA accessibility. Interestingly, despite their architectural role, H1 histones were shown to be highly mobile and continuously exchanging among chromatin-binding sites (Raghuram et al., 2009). They are also the most variable of the histones, with numerous nonallelic variants coexisting in the same cell. In vertebrates, several evolutionarily conserved subfamilies of H1 can be distinguished (Talbert et al., 2012) and appear to play both redundant and specific roles during development and cellular differentiation (McBryant et al., 2010). There is accumulating evidence that, in animals, regulation of the proportions of H1 variants with different dynamic behavior in chromatin is involved in controlling the accessibility of DNA to trans-acting factors (Jullien et al., 2010; Shahhoseini et al., 2010; Zhang et al., 2012a; Pérez-Montero et al., 2013; Christophorou et al., 2014).

Epigenetic mechanisms, including DNA and histone modifications and active nucleosome remodeling, are major players in translating signals about environmental perturbations into adaptive responses at the transcriptional

level (Smith and Workman, 2012; Kinoshita and Seki, 2014). In the last decade, considerable progress has been made in understanding the function of H1 in shaping chromatin epigenetic signatures (Harshman et al., 2013). Importantly, in both plants and animals, H1 histones are involved in maintaining the pattern of DNA methylation (Fan et al., 2005; Wierzbicki and Jerzmanowski, 2005; Zemach et al., 2013). As suggested by these studies, H1 is most likely a major regulator of the accessibility of chromatin to DNA methyltransferases. It was also shown to be involved in chromatin reprogramming during the somatic-to-reproductive cell fate transition in Arabidopsis (*Arabidopsis thaliana*; She et al., 2013).

Plant H1s can be divided into ubiquitously and stably expressed major (main) variants and stress-inducible minor variants (Jerzmanowski et al., 2000; Talbert et al., 2012). The minor variants subfamily is evolutionarily conserved and ancient, since it appeared before the split into monocotyledonous and dicotyledonous plants (Jerzmanowski et al., 2000). The model plant Arabidopsis has three nonallelic H1s: the highly similar major variants H1.1 and H1.2 and a single stress-inducible minor variant H1.3 (Jerzmanowski et al., 2000).The occurrence of the stress-inducible linker histones was discovered when an *H1-D* gene in the wild tomato *Solanum pennellii* was identified and shown to be strongly induced by drought stress and abscisic acid (ABA; Cohen and Bray, 1990; Cohen et al., 1991; Plant et al., 1991; Wei and O'Connell, 1996). Close homologs were subsequently identified in other plant species (e.g. Arabidopsis and tobacco [*Nicotiana tabacum*]) and shown to be induced by similar conditions (Ascenzi and Gantt, 1997; Przewloka et al., 2002).

Importantly, immunostaining of whole nuclei with specific antibodies showed that the distribution of H1.3 differed from that of H1.1 and H1.2 (which was identical), suggesting that H1.3 binds to different genomic regions compared with the main H1 variants (Ascenzi and Gantt, 1999b). Arabidopsis, wild tomato, and tobacco plants with down-regulation of the stress-inducible linker histone variant do not show defects in development and global chromatin organization under normal conditions (Ascenzi and Gantt, 1999a; Scippa et al., 2000, 2004; Przewloka et al., 2002), suggesting that this group of linker histones has no major role in the basal functions of plant development or in chromatin structure. However, the tomato (*Solanum lycopersicum*) homolog H1-S has been implicated in maintaining the water status during a specific window in drought treatment. Transgenic tomato plants with down-regulated H1-S showed increased stomatal conductance, transpiration, and photosynthetic rate compared with wild-type plants, consistent with a role for this protein in regulating stomatal function (Scippa et al., 2004).

In contrast to tomato, the depletion of stress-inducible H1 variants in wild tomato and in Arabidopsis was not accompanied by observable changes in the drought response (Wei and O'Connell, 1996; Ascenzi and Gantt, 1999a), so the biological role of these proteins remains unclear. Nevertheless, the sequence homology of the drought stress-inducible variants, and the fact that, unlike other known histone genes, they can be regulated by environmental factors, lend support to the suggestion that these H1 variants may play some special role in the regulation of gene expression.

Here, we used previously unavailable molecular and genetic tools to address the following questions. (1) How are Arabidopsis linker histones distributed in the plant under normal and stress conditions? (2) Are there environmental conditions under which H1.3 becomes a limiting factor to adaptive responses? (3) Where and how does H1.3 bind in the genome under normal and stress conditions? (4) Is there a functional link between its binding properties and cellular reprograming during physiological responses to stress?

We show that prolonged growth in low light leads to robust induction of H1.3 protein, which enables in-depth characterization of the entire complement of linker histones in Arabidopsis under both normal and stress conditions, including their in vivo binding properties and global occupancy profiles along chromosomes. We further establish that stress-inducible H1.3 is represented in Arabidopsis by two independent pools: one constitutive,

[1] This work was supported by the Institute of Biochemistry and Biophysics, Polish Academy of Sciences, and the University of Warsaw; the European Cooperation in Science and Technology (grant no. MNiSW 212/N–COST/2008/0 to A.J.); the Ministry of Science and Higher Education (grant no. MNiSW/PO4A/03928 to A.J., grant no. MNiSW/NN301/269237 to K.R. and S.S., grant no. MNiSW/NN301/033234 to M.P., grant no. MNiSW/NN301/201539 to J.H.-P., and grant nos. PBZ–MNiI–2/1/2005 and MNiSW/NN301/469138 to M.K.); the Foundation for Polish Science (grant no. TEAM/2010–6 to K.G.); the National Science Centre (grant no. 2011/02/A/NZ2/00014 to K.G.); the National Centre for Research and Development (grant no. PBS1/A9/16/2012 to K.G.); the University of Agriculture in Cracow (grant no. DS3113/KFR/2012–14 to M.R., K.Ś.Ś., J.K., and K.Ż.); the Estonian Research Council (grant no. IUT2–21 to H.K.); and the European Regional Fund (CoE Environ grants to H.K.).

[2] Present address: Institute of Plant Biology, University of Zurich, Zollikerstrasse 107, CH–8008 Zurich, Switzerland.

[3] Present address: Laboratory of Preclinical Testing of Higher Standard, Nencki Institute of Experimental Biology, Pasteura 3, 02–093 Warsaw, Poland.

* Address correspondence to andyj@ibb.waw.pl.

The author responsible for distribution of materials integral to the findings presented in this article in accordance with the policy described in the Instructions for Authors (www.plantphysiol.org) is: Andrzej Jerzmanowski (andyj@ibb.waw.pl).

A.J., K.R., and M.R. conceived the original screening and research plans; M.Kob., K.G., S.S., H.K., M.R., J.T., and P.Z. supervised the experiments; K.R., M.P., J.H.-P., M.L., M.A.K., R.A., L.K., R.I.-N., K.Ś.-Ś., J.K., K.Ż., F.J., K.L.-K., and I.J. performed most of the experiments; A.J., K.R., M.R., B.W., B.L., A.M., M.Kot., K.G., P.S., R.A., K.B., A.F., M.Kob., and H.K. designed the experiments and analyzed the data; A.J. and K.R. conceived the project and wrote the article with contributions of all the authors; M.R. supervised and complemented the writing.

[OPEN] Articles can be viewed without a subscription.
www.plantphysiol.org/cgi/doi/10.1104/pp.15.00493

confined to guard cells, and the other facultative, occurring in other tissues, which is controlled by environmental cues. Furthermore, we show that H1.3 is required for both stomatal functioning under normal growth conditions and for adaptive developmental responses to complex environmental stress of combined light and water deficiency. In addition, the depletion of H1.3 abolishes a substantial part of stress-related DNA methylation. Taken together, our findings suggest that H1.3 mediates adaptive responses to complex environmental stress via global alteration of chromatin properties, which favors reprogramming of the epigenetic landscape and gene expression.

RESULTS

Prolonged Growth of Arabidopsis under a Low-Light Regime Leads to the Robust Induction of H1.3 Protein in Most Tissues

The limited repertoire of linker histone variants makes Arabidopsis an ideal model in which to study the possible adaptive role of the stress-inducible H1s in plants. To assess the distribution of H1 variants in a tissue-specific manner, we used transgenic lines expressing H1-GFP fusion proteins under the control of their native promoters. H1.1 and H1.2 fused to GFP were detected in all vegetative tissues and organs, while the H1.3-GFP line was observed almost exclusively in guard cells (Fig. 1A). This is consistent with the findings of an earlier study using transcriptional fusions (Ascenzi and Gantt, 1999a) and with transcriptome analyses showing that *H1.3* is one of the most highly expressed transcripts in guard cells (Leonhardt et al., 2004).

When we compared *H1.3* expression in plants subjected to different environmental stresses (data not shown), we found that reduced light intensity during the day induced a remarkable global increase in H1.3-GFP in shoot and root tissues (Fig. 1A). Under these conditions, H1.3 appeared coexpressed in the same cells as the H1.1 and H1.2 variants (Fig. 1A). The low-light conditions we used were reported previously to cause

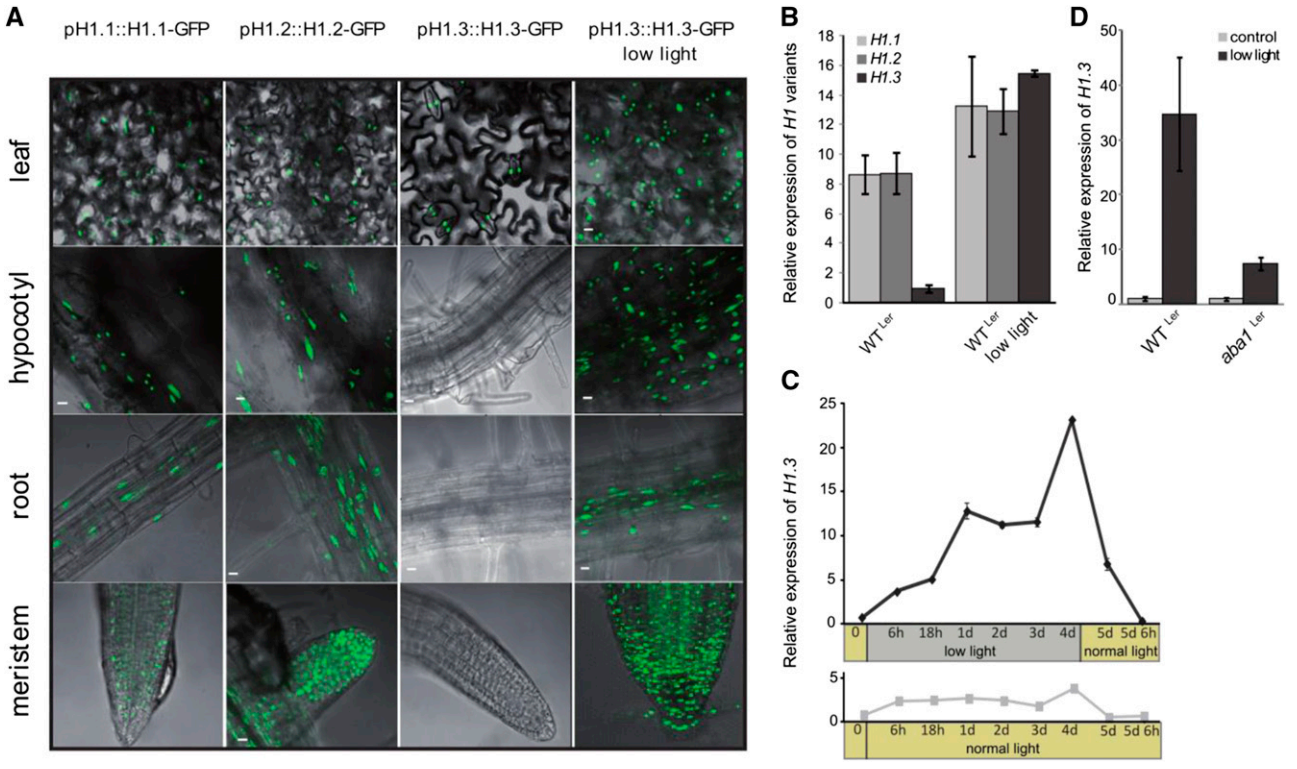

Figure 1. H1.3 is induced by prolonged low-light treatment in an ABA-dependent manner. A, Distribution of Arabidopsis H1s in different tissues shown by the green fluorescence of GFP-tagged forms. The locations of H1.1, H1.2, and H1.3 fusion proteins are shown in control conditions, while the H1.3 protein distribution is also shown after 4 d of low-light treatment. Bars = 10 μm. B, Relative expression (reverse transcription-quantitative PCR [RT-qPCR]) of *H1* proteins in wild-type (WT^{Ler}) plants in control conditions and after low-light treatment (expression of *H1.3* in the wild type under normal conditions = 1). The plotted values are means ± SD for replicates consisting of four plants grown in soil. C, Relative expression of *H1.3* during growth in low light for 4 d followed by transfer back to control conditions. Yellow bars indicate control conditions, and the gray bar indicates the low-light period. The plotted values are means ± SD for replicates consisting of approximately 35 plants grown on Murashige and Skoog agar plates. D, Relative expression of *H1.3* in *aba1* plants after 4 d of low-light treatment. The plotted values are means ± SD for replicates consisting of four plants grown in soil. All quantitative reverse transcription-PCR measurements were normalized to the expression of *Ubiquitin C* (*UBC*).

reduction in chromatin compaction (van Zanten et al., 2010). At the transcript level, *H1.3* showed an increase of 10- to 35-fold from its basal level in noninduced plants, depending on the age of the plant and probably other uncontrolled factors (Fig. 1B; Supplemental Fig. S1A). This is consistent with the results of genome-wide expression profiling experiments, including data from dedicated large-scale projects, and online tools like Genevestigator (Zimmermann et al., 2004) and AtGenExpress (Schmid et al., 2005; Kilian et al., 2007), showing that the expression of *H1.3* is characterized by exceptionally high-amplitude fluctuations in roots, stems, and leaves, depending on growth conditions, developmental stage, and differentiation level (Supplemental Fig. S2). The induction of *H1.3* was equally effective in both the Landsberg *erecta* (L*er*) and Columbia-0 (Col-0) ecotypes (Supplemental Fig. S1, A and B). Importantly, the effect of low light on the expression of *H1.3* was significantly stronger than that of complete darkness (Supplemental Fig. S1C). The systemic induction of H1.3-GFP required 3 to 4 d of low light. Moreover, within 1 to 2 d after restoring standard light conditions, *H1.3* expression, as determined by transcript abundance, had returned to its normal low level (Fig. 1C).

The *H1.3* transcript is up-regulated in response to ABA treatment (AtGenExpress; Supplemental Fig. S1D). To determine whether *H1.3* induction under low light depends on the ABA signaling pathway, we examined the level of *H1.3* mRNA in the ABA-deficient *aba1* mutant grown in low light. On average, *H1.3* transcript levels in the mutant were 5-fold lower than those in wild-type plants (Fig. 1D), indicating that *H1.3* expression strongly depends on the ABA signaling pathway. This is consistent with the presence of ABA-responsive elements close to the transcription start site in the *H1.3* promoter (Supplemental Fig. S3; Berendzen et al., 2006; Gómez-Porras et al., 2007; Fujita et al., 2011). Interestingly, an autonomous ABA biosynthesis pathway in guard cells was recently discovered (Bauer et al., 2013), and this could account for the stable occurrence of H1.3 in these highly specialized cells. In contrast to ABA deficiency, the absence of the main photoreceptors (Phytochrome A [PhyA]/PhyB and Cryptochrome1 [Cry1]/Cry2) not only did not inhibit, but slightly enhanced, the induction of *H1.3* by low light (Supplemental Fig. S1E), suggesting their possible negative role in low light-induced *H1.3* expression in wild-type plants. Interestingly, H1.3 was recently shown to belong to a narrow group of 39 genes comprising a core response module with a critical role in retrograde plastidial-to-nucleus signaling (Glasser et al., 2014). Thus, its up-regulation could be the result of complex secondary effects (including, but not restricted to, an increase in ABA) of the change in redox levels due to reduced photosynthetic activity (Pfalz et al., 2012). This is consistent with the relatively small role in *H1.3* regulation of the major photoreceptors, which are known to play only a minor function in retrograde signaling (Fey et al., 2005; Lepistö et al., 2012).

Lack of H1.3 Affects Stomatal Functions and Development

In order to assess the role of H1.3 in Arabidopsis physiological responses, we used *h1.3* null mutants (Supplemental Fig. S4) in parallel with their sibling wild-type plants. To examine plant responses to conditions closely resembling those occurring naturally, where light fluence on a moderately cloudy summer day is in the range of 350 to 450 μmol m^{-2} s^{-1}, we studied plants grown in 400 rather than 150 μmol m^{-2} s^{-1} light fluence (standard for laboratory experiments with Arabidopsis). We also assumed that any differences between control and low-light conditions would be observed more readily when the change in light fluence was an increase rather than a decrease. Using the H1.3-GFP line, we first confirmed that the H1.3 protein was not induced by the raised light fluence and was only visible in guard cells, similar to Figure 1. Wild-type and *h1.3* plants grown under high-light conditions were similar in size (Supplemental Tables S1 and S2), but the mutant plants were characterized by a reduced CO_2 assimilation rate per plant (Fig. 2A) and a decreased stomatal density in young leaves, especially in the upper epidermis (Fig. 2B; Supplemental Fig. S5A). This suggested a role for H1.3, not only in the regulation of stomatal functioning, in accordance with an earlier report (Scippa et al., 2004), but, unexpectedly, also in their development. To determine whether the above differences were reflected at the level of gene transcription, we compared the transcriptomic profiles of wild-type and *h1.3* plants in control conditions using Agronomics microarrays and found that nearly 10% of genes were differentially expressed in the mutant, although most of the observed changes in gene expression were moderate (Supplemental Data Set S1). Interestingly, the proportion of genes showing altered expression (categorized as differentially expressed at fold change [Fch] > 1.5 and $P < 0.05$) due to H1.3 depletion was highest (almost 30%) among those reported to be preferentially expressed in guard cells (Fig. 2C). Moreover, the depletion of H1.3 significantly affected the expression of key genes involved in stomatal development, including *SPEECHLESS* (*SPCH*), *MUTE*, *FAMA*, *ERECTA-family/TOO MANY MOUTHS*, and *MKK9*, encoding a mitogen-activated protein kinase (Fig. 2D). These genes are not expressed in mature guard cells but in different developmental phases of the stomatal lineage, including the meristemoid cell, a stem cell-like stomatal precursor (Lau and Bergmann, 2012). Most of these genes, with the exception of *MKK9*, which was up-regulated, were down-regulated in parallel with the decrease in stomatal density in the *h1.3* mutant (Fig. 2B). Interestingly, the loss-of-function *spch* mutants lacked stomata on the leaf epidermal surfaces and died early (MacAlister et al., 2007). However, in contrast to the null mutant, the expression of *SPCH* in the *h1.3* mutant, albeit low, was clearly detectable. There is no proof of a linear relationship between *SPCH* transcript and protein levels; on the contrary, Arabidopsis was shown to have an efficient system controlling

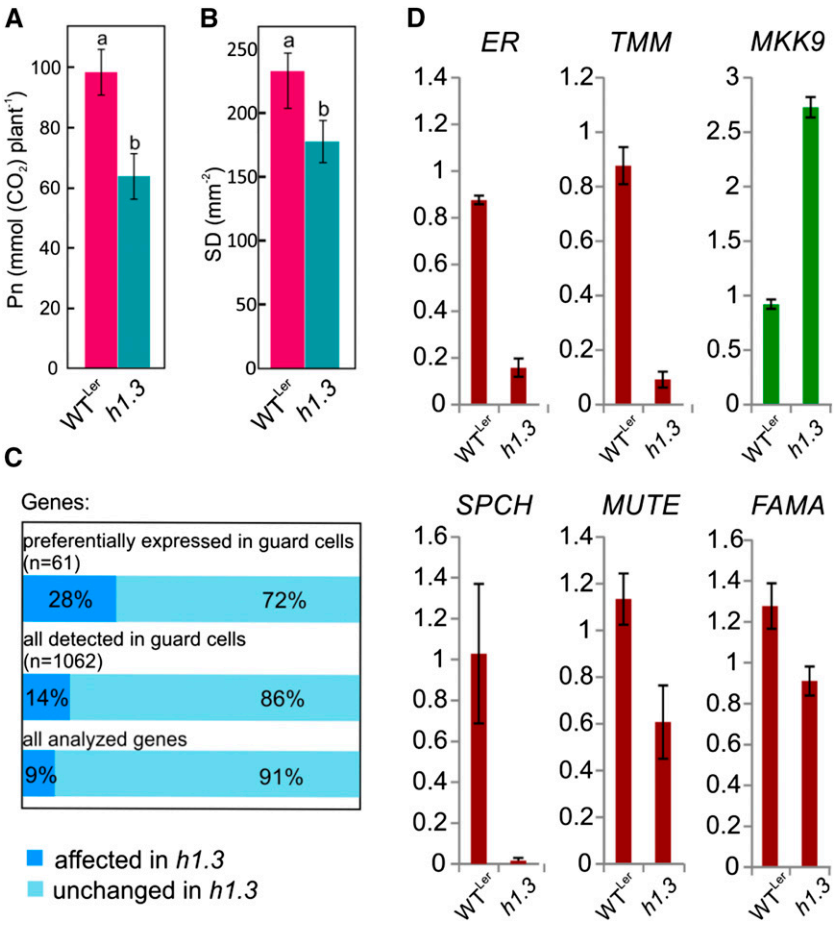

Figure 2. H1.3 influences stomatal functioning and biogenesis. A and B, Effects of a lack of H1.3 on CO_2 net assimilation rate (Pn; A) and stomatal density (SD; B). The differences between CO_2 net assimilation rate and stomatal density values marked with different letters are statistically significant ($P < 0.05$, Tukey's honestly significant difference test). C, Expression of genes specific for guard cells in *h1.3*. Color bars indicate the percentage of genes showing altered (blue) or unchanged (light blue) expression in *h1.3*, divided into two different classes: preferentially expressed only in guard cells ($n = 61$) and all expressed in guard cells ($n = 1{,}063$), classified as described previously (Leonhardt et al., 2004). The following criteria were met by all affected genes in *h1.3*: Fch > 1.5 and $P < 0.05$. D, Relative expression (RT-qPCR) of genes with key functions in guard cell biogenesis in *h1.3* mutant and wild-type (WT^{Ler}) plants. All quantitative reverse transcription-PCR measurements were performed for at least three replicates and were normalized to the expression of *UBC*.

SPCH abundance (Kumari et al., 2014), highlighting the importance of posttranscriptional regulation in this case. It is thus plausible that the level of the *SPCH* transcript detected in the *h1.3* mutant was still sufficient for the induction of stomata, although at decreased density, as shown in Figure 2B.

After normalization of the expression values against the number of stomata, the overall pattern was similar to that before normalization: the expression of *ERECTA*, *TOO MANY MOUTHS*, and *SPCH* was lower and that of *MKK9* was higher in the *h1.3* mutant than in the wild type. However, there was no difference between the mutant and wild-type plants in the expression of *FAMA* and *MUTE*, suggesting that the reduced expression of these two genes may result from lowering the number of stomata (Supplemental Fig. S5B).

Taken together, our results are consistent with the notion that H1.3 acts as a regulator of stomatal functions. Further studies are required to determine whether the significant changes in the transcription of key genes regulating stomatal development from precursor cells, observed in the *h1.3* mutant, are due to the direct effect of H1.3 on these genes or are an indirect effect of impaired stomatal physiology in early development that leads to altered stomatal development in young leaves.

H1.3 Is Required for the Reduction of Arabidopsis Growth in Response to Combined Low-Light/Drought Treatment

Stress-inducible H1s are up-regulated by drought (Ascenzi and Gantt, 1997; Scippa et al., 2000), and the effects of RNA interference-mediated down-regulation of a tomato homolog of H1.3 suggested that they may promote plant sensitivity to water stress (Scippa et al., 2004). A comparison of the efficiency of limited drought and low light in inducing *H1.3* expression showed that 17 d of water limitation was as effective as the same period of low light in inducing the accumulation of *H1.3* mRNA. Surprisingly, levels of this transcript increased synergistically when the two stresses were combined (Fig. 3A), suggesting that plants responded to this combination of stresses in a synergistic manner. All plants were subjected to soil water deficit under both low- and high-fluence light conditions, and different morphological and physiological parameters were assessed (Fig. 3, B–D; Supplemental Tables S1 and S2).

The normal reaction of Arabidopsis to water limitation is growth retardation, resulting mainly from decreased biomass accumulation after stomatal closure under mild drought conditions and more rapid generative development (Chaves et al., 2009). A graph of the

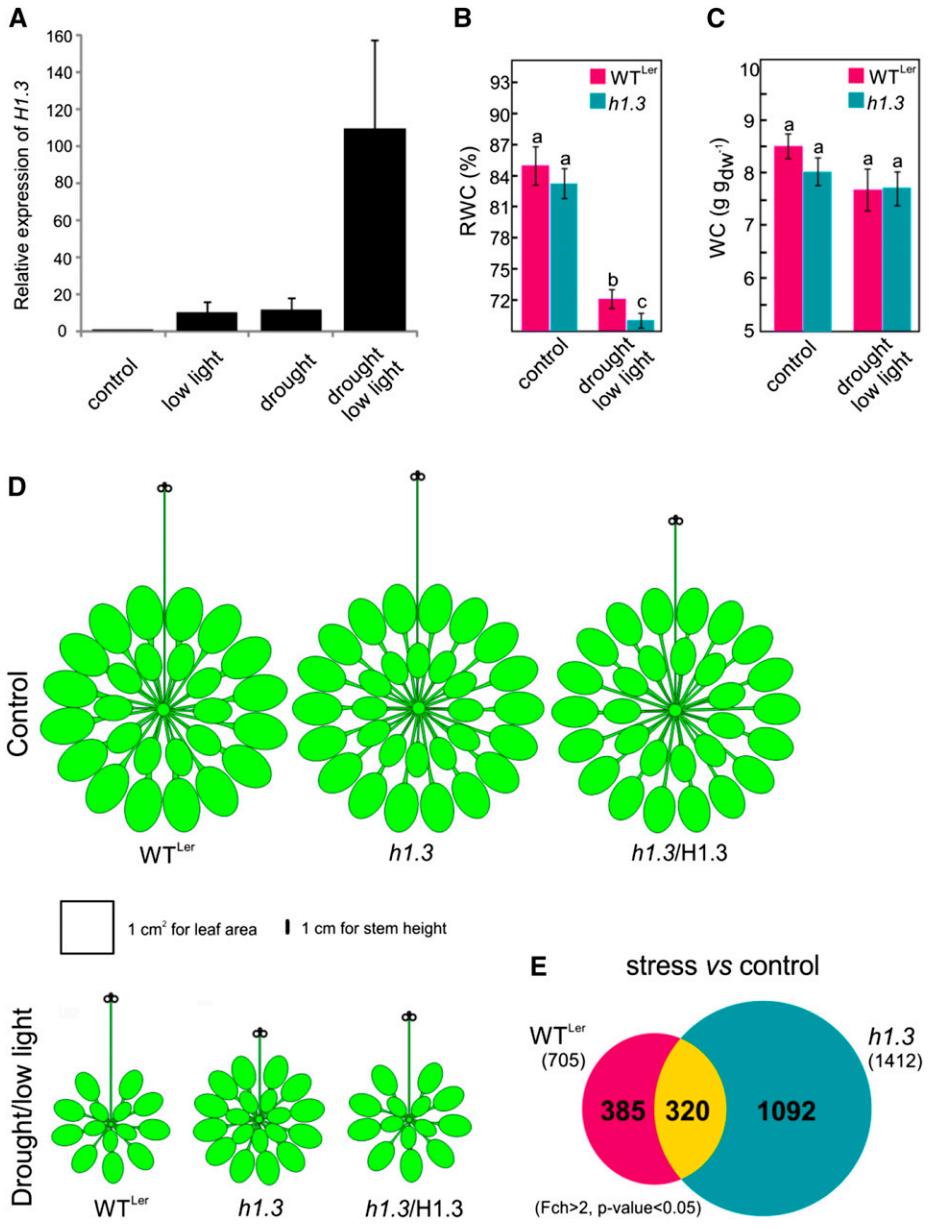

Figure 3. H1.3 plays a critical role in developmental and physiological responses of Arabidopsis to environmental stresses. A, Relative expression of *H1.3* (RT-qPCR) after 17 d of low-light, drought, and drought in low-light conditions. RT-qPCR measurements were performed for at least three replicates and were normalized to the expression of *UBC*. B and C, Effects of low-light/drought treatment on relative leaf water content (RWC; B) and absolute leaf water content (WC; C). The differences between RWC and WC values marked with different letters are statistically significant ($P < 0.05$, Tukey's honestly significant difference test). D, Diagrammatic representation of the phenotype (adult plant morphology and size) in control conditions and in response to drought under limited light conditions of the wild type (WT^{Ler}), *h1.3*, and complemented *h1.3* mutant (*h1.3*/H1.3). Scales are as shown. E, Venn diagram showing the number of genes with altered expression in response to low-light/drought conditions in the wild type (red), *h1.3* (blue), and both genotypes (yellow). The expression pattern of selected genes was verified by RT-qPCR (Supplemental Figs. S9 and S10).

average quantitative phenotype confirmed our earlier observation that wild-type and *h1.3* null plants were morphologically indistinguishable when grown in control conditions (Fig. 3D). However, in combined low light/drought, the *h1.3* plants had a higher leaf number and increased dry and fresh weights compared with wild-type plants, irrespective of the growth stage at which they were subjected to drought (Fig. 3D; Supplemental Figs. S6 and S7; Supplemental Tables S1 and S2). Stem formation and flowering under low-light/drought stress occurred more slowly in *h1.3* plants than in wild-type plants. The *h1.3* plants showed not only an increased growth rate compared with wild-type plants but also a higher net photosynthetic rate (Supplemental Tables S1 and S2) and lower RWC in their leaves (Fig. 3B). Interestingly, the WC per dry weight in drought was similar in the wild-type and *h1.3* plants (Fig. 3C). This suggested that the observed changes in RWC resulted from differences in the accumulation of osmolytes in the leaf cells. The stomatal density in the lower epidermis of *h1.3* plants decreased only 2-fold in low-light/drought conditions, compared with a 4- to 5-fold decrease in wild-type plants. In the *h1.3* mutant, the stomatal density, while lower in control conditions, was higher under low light/drought than in wild-type plants (Supplemental Fig. S5), which is indicative of the decreased ability of *h1.3* plants to adjust stomatal biogenesis to environmental conditions (Fig. 2). While it is likely that differences in the photosynthetic rate and RWC caused by low light/

drought were mostly due to changes in stomatal activity, nonstomatal factors cannot be ruled out. The differences in the growth retardation effect of low light/drought (Fig. 3D) could be due to changes in the leaf ABA content; however, we found similar ABA levels in *h1.3* and wild-type plants (Supplemental Fig. S8). This points to differences in downstream ABA targets as the possible cause of the observed phenotypes. Importantly, all of the physiological and developmental effects of the *h1.3* mutation in plants under stress described above were not observed in mutant plants complemented with H1.3-GFP, which reacted similarly to the wild type (Fig. 3D; Supplemental Fig. S7; Supplemental Tables S1 and S2).

In natural conditions, the inability to restrict growth and photosynthetic rate under prolonged low-light/drought stress confers only a very short-term advantage. In the longer term, it obviously impairs a common adaptive strategy of plants under such conditions (i.e. restriction of metabolism and growth, leading to delayed reproduction) aimed at minimizing the loss in fitness. To better understand the molecular basis of the observed *h1.3* phenotype, we performed global transcriptome profiling. Exposure of wild-type Arabidopsis to mild drought and low-light conditions induced strong transcriptional reprogramming. The genes that were most affected included those classified as responsive to stress, hormones, and environmental stimuli and those connected with lipid and cell wall functions (Supplemental Data Set S2; agriGO [Du et al., 2010]). Importantly, the response of *h1.3* mutants during stress differed considerably from that of wild-type plants (Fig. 3E; Supplemental Data Sets S2 and S3). In response to the imposed environmental changes, wild-type plants showed altered expression of about 705 genes (Fch ≥ 2, $P < 0.05$), whereas the transcript levels of twice that number of genes (1,412) were changed in the *h1.3* mutant, with only 23% of these in common with the wild type (Fig. 3E). When interpreting these differences, it should be remembered that, under control conditions, wild-type and *h1.3* plants differ in their expression of about 10% of all genes, many of which play a critical role in stomatal biogenesis and function (Supplemental Data Set S2). It is possible that this major primary difference could lead to amplified secondary differences under stress conditions.

Comparison of the transcriptomic profiles of wild-type and *h1.3* mutant plants grown under stress conditions revealed that, in the absence of H1.3, 70% of the affected transcripts were down-regulated (Fch > 1.5, $P < 0.05$), and this value increased to 82% for an Fch of greater than 3, while in control conditions, the equivalent proportions of down-regulated transcripts were 58% for an Fch of greater than 1.5 and 53% for an Fch of greater than 3 (Supplemental Data Sets S1 and S4). This suggests that, under conditions of stress, H1.3 acts mainly as a positive rather than a negative regulator of gene transcription.

H1.3 Binds Chromatin with Considerably Higher Dynamics Than the Main H1 Variants

In guard cells of nonstressed plants, H1.1, H1.2, and H1.3 showed different mobilities, with half-time recovery ($t_{1/2}$) of 6.8, 16.8, and 3.4 s and stable bound pools of 28%, 14%, and 3%, respectively. Interestingly, the characteristics of H1.2 resembled those of H2B ($t_{1/2}$ of 14.8 s, 78% stable pool). These data showed that H1.3 is the most dynamic variant and probably occurs as a pool of rapidly diffusing molecules (Fig. 4; Supplemental Videos S1–S3).

We next compared H1 mobilities in the nuclei of root, hypocotyl, and root meristem cells under control and low-light growth conditions. H1.2 showed the lowest mobility in all analyzed tissues ($t_{1/2}$ of approximately 22

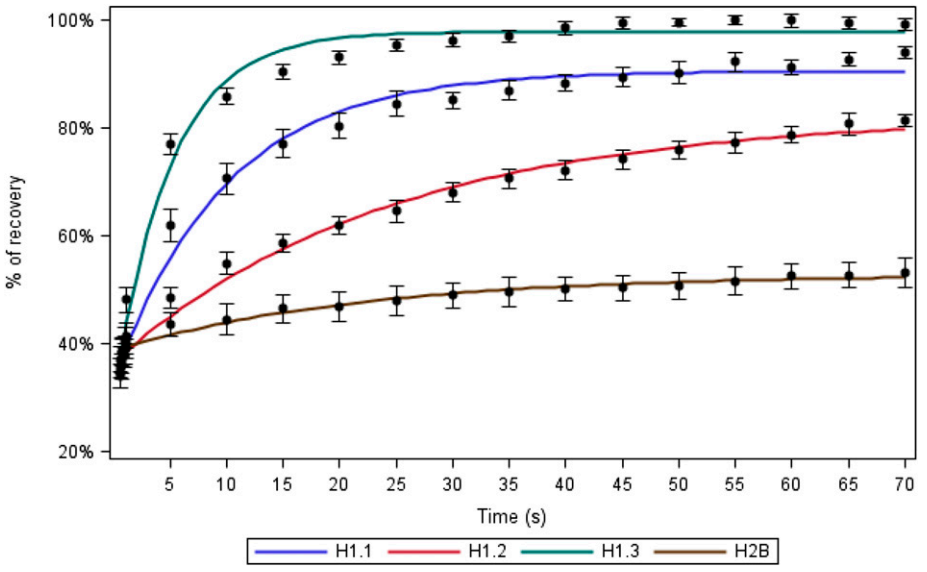

Figure 4. Main and stress-inducible H1s have different in vivo chromatin-binding properties. Fluorescence recovery after photobleaching (FRAP) analyses are shown for GFP-tagged H1 variants and H2B in guard cells of unstressed plants. The data show the percentage of fluorescence recovery from 0 to 70 s after photobleaching. Note that 70 s does not encompass the full recovery of fluorescence for H1.1, H1.2, and H2B. Errors bars indicate SD ($n = 7$, 9, 11, and 4 nuclei for H1.1, H1.2, H1.3, and H2B, respectively).

s), indicative of the strongest interaction with chromatin. The low light-induced H1.3 consistently showed the highest mobility ($t_{1/2}$ of approximately 2–3 s). The binding properties of H1.1 ($t_{1/2}$ of 6.2–16.2 s) were more similar to H1.2 than to H1.3. In all three analyzed organs, the recovery of H1.2 was on average 30% faster in low light than in control conditions, which is consistent with its weaker interaction with chromatin after prolonged low-light stress (Table I). Moreover, the faster overall exchange of H1.2 in low light was mostly due to a significant increase in recovery during the first few seconds after photobleaching (data not shown), which is indicative of an increased soluble or loosely bound pool in this initial phase (Phair et al., 2004). The mobility of H1.1 in low light changed to a lesser extent (9%–16%) and increased only in root and meristem, whereas it decreased in hypocotyl (Table I). The observed differences in histone mobilities among tissues, as measured by FRAP, are characteristic of cell differentiation and development in Arabidopsis and are probably due to changes in the global chromatin states (Rosa et al., 2014).

To summarize, we have demonstrated that H1.3 has no stable bound pool in the nucleus and exchanges in chromatin extremely rapidly. These properties may be caused by conserved amino acid replacements in the H1.3 GH1 binding sites S1 and S2 as well as the shortening of its C-terminal domain (CTD; Supplemental Fig. S11). Interestingly, the appearance in evolution of stress-inducible H1s seems to coincide with the onset of angiosperms (Supplemental Figs. S12–S14).

Mapping the Genome-Wide Distribution of H1 Variants Reveals Differences in Their Preferences for Epigenetic Marks of Active and Repressive Chromatin

The differences in the GH1 binding sites and CTD, and in vivo chromatin dynamics between the main linker histone variants and H1.3, prompted us to ask whether these two types of H1 also differ in their chromatin localization preferences. We used our H1-GFP-tagged lines and chromatin immunoprecipitation (ChIP)-on-chip technology to analyze the distribution of all three H1 variants in Arabidopsis plants grown in low light or in control conditions. Initially, we looked at overall patterns of H1 distribution among different types of sequences. Both the main and stress-inducible H1s were generally depleted in introns and 5′ untranslated regions (UTRs) compared with exons, 3′ UTRs, and transposons (Fig. 5A; Supplemental Fig. S15; Supplemental Table S3). Interestingly, the magnitude of the enrichment compared with the total genome signal of the stress-inducible H1.3 to the main variants was markedly decreased on transposons compared with total genic regions or exons and 3′ UTRs (Fig. 5A; Supplemental Fig. S15; Supplemental Table S3).

Next, we analyzed the qualitative profiles of the main H1 variants and the core histone H3 along the chromosomes of Arabidopsis grown in control and low-light conditions and compared these with the H1.3 profile after its induction by low light. All three H1 variants were found to be enriched in pericentromeric regions (resembling the distribution pattern of heterochromatic transposons; Lippman et al., 2004) but not in the central region of the centromere, where the signal for the core histone H3 was close to its maximum level (Supplemental Fig. S16). Importantly, while the intensity profiles for H1.1 and H1.2 along chromosomes were strongly correlated, independently of the growth conditions (Pearson's $r = 0.97$), the profile for H1.3 after its induction by low light was notably less correlated with those of the main variants (Pearson's $r = 0.81$ and 0.74, respectively). This suggests that, despite their likely similar specificity for nucleosomal sites, the chromosome-wide occupancy of the main linker histone variants and H1.3 may be governed by different preferences for some additional feature(s) of these sites. This is consistent with an earlier report demonstrating that, while H1.1 and H1.2 antibodies decorate nuclei in patterns very similar to 4′,6-diamino-2-phenylindole staining, antibodies raised against H1.3 bind to

Table I. *Summary of* $t_{1/2}$ *and percentages of mobile fraction for histone-GFP constructs measured in control and low-light conditions*

$t_{1/2}$ and mobile fraction were calculated based on the estimation of parameters of the adopted FRAP model (see "Materials and Methods"). For each plant organ, histone dynamics were measured in control and stress conditions. All values are averages of at least four sets of single-cell FRAP data (the number of cells is shown in parentheses). High and low values of $t_{1/2}$ indicate low and high protein mobility, respectively. Mobile fraction indicates the percentage of the total protein pool not involved in stable interactions with chromatin. The presented values reflect characteristics of histone mobility during the first 70 s of the experiment. For histones whose fluorescence intensity does not reach a plateau within 70 s (Fig. 4), extending the time of measurement could result in higher $t_{1/2}$ and lower mobile fraction estimates. A dash indicates that the parameters were not measured.

Treatment	Histone	$t_{1/2}$				Mobile Fraction			
		Root	Hypocotyl	Meristem	Leaf	Root	Hypocotyl	Meristem	Leaf
		s				%			
Control	H1.1	12.2 ± 0.8 (2)	6.2 ± 0.6 (2)	16.2 ± 1.3 (4)	6.8 ± 0.5 (7)	73.9 ± 1.9 (2)	91.1 ± 3.4 (2)	63.7 ± 2.0 (4)	86.1 ± 2.4 (7)
	H1.2	21.3 ± 1.8 (10)	21.1 ± 1.3 (7)	22.3 ± 4.0 (4)	16.8 ± 1.2 (9)	43.0 ± 1.5 (10)	77.9 ± 2.0 (7)	29.5 ± 2.2 (4)	72.3 ± 2.0 (9)
	H1.3	–	–	–	3.4 ± 0.3 (11)	–	–	–	97.1 ± 3.4 (11)
	H2B	25.7 ± 4.4 (6)	23.5 ± 5.2 (6)	13.1 ± 2.6 (10)	14.8 ± 1.9 (4)	64.8 ± 5.0 (6)	35.3 ± 3.4 (6)	38.5 ± 2.7 (10)	23.1 ± 1.1 (4)
Stress	H1.1	10.3 ± 0.8 (11)	8.5 ± 0.5 (8)	15.2 ± 0.8 (10)	8.4 ± 0.5 (5)	72.4 ± 2.0 (11)	86.0 ± 1.9 (8)	71.1 ± 1.4 (10)	86.3 ± 2.1 (5)
	H1.2	15.6 ± 1.0 (10)	15.1 ± 0.6 (5)	14.8 ± 2.2 (7)	19.4 ± 1.3 (6)	73.3 ± 1.7 (10)	80.2 ± 1.2 (5)	23.1 ± 1.2 (7)	74.4 ± 2.0 (6)
	H1.3	2 ± 0.3 (10)	1.3 ± 0.2 (6)	1.0 ± 0.1 (5)	3.0 ± 0.2 (13)	99.7 ± 6.7 (10)	100.0 ± 10.0 (6)	99.8 ± 10.7 (5)	100.0 ± 2.6 (13)
	H2B	24.9 ± 4.2 (10)	12.2 ± 0.8 (6)	29.4 ± 5.1 (9)	23.6 ± 3.1 (5)	48.6 ± 3.7 (10)	33.3 ± 0.8 (6)	47.3 ± 4.0 (9)	47.4 ± 2.7 (5)

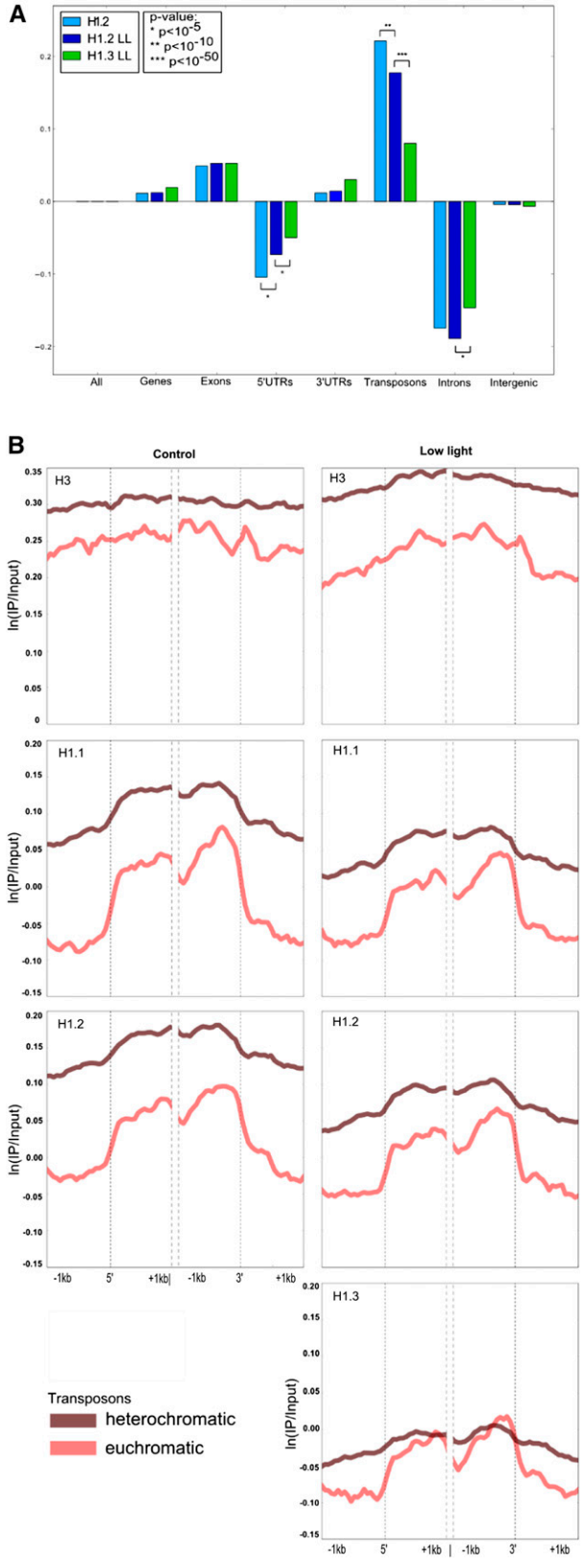

Figure 5. Genomic distribution of H1 variants. A, Genomic profiles of H1.2 and H1.3 in control conditions and after 4 d of low-light (LL) treatment. The length of the colored bars represents enrichment or depletion compared with the total genome signal. H1.1 has a similar profile to H1.2 (Supplemental Fig. S15). Only the depletion of H1s in intergenic regions and enrichment in 3′ UTRs are not statistically significant (Supplemental Table S3). Asterisks indicate significant differences between H1.2 occupancy in control and low-light conditions and between H1.2 and H1.3 in low-light conditions. B, Average distribution of the main H1 variants, H1.3 and H3, in control and low-light conditions around the 3′ and 5′ ends (±1 kb) of transposons located in heterochromatin and euchromatin (differentiated by the level of H3K9me2 occupancy). IP, Immunoprecipitate.

chromatin in a diffuse pattern distinct from 4′,6-diamino-2-phenylindole staining (Ascenzi and Gantt, 1999b).

The relative abundance of the main H1 variants was higher on heterochromatic compared with euchromatic transposons (Fig. 5B), resembling the preferences reported for mammalian somatic H1s (Cao et al., 2013; Izzo et al., 2013). In contrast, the abundance of low light-induced H1.3 appeared similar on the two transposon types (Fig. 5B). Interestingly, low-light treatment led to a decreased relative abundance of H1.1 and H1.2 on the 5′ and 3′ ends of both heterochromatic and euchromatic transposons. Together, these characteristics are consistent with the possibility that, while H1.3 generally competes with the main H1 variants for the same binding sites, its effects may be more pronounced in a specific subset of these sites.

We next compared the distribution of the nucleosomal core histone H3 and the H1 variants on genes with different transcriptional activity (Fig. 6). H3 mapping showed a typical well-positioned +1 nucleosome at the right border of the 5′ nucleosome-depleted region (NDR), coinciding approximately with the TSS. In accordance with data for other organisms (Jiang and Pugh, 2009), this pattern was most distinct for Arabidopsis genes with the highest transcriptional activity. The signals for all three H1 variants showed identical profiles, consistent with their ability to bind to the same sites. Interestingly, the inverse correlation between occupancy by H1 and the level of gene expression was weaker for H1.3 than for H1.1 and H1.2, suggesting that the presence of the former is less associated with actual transcriptional activity. While H3 was depleted in 5′ and 3′ NDRs and remained at a relatively stable level throughout gene bodies, the H1s were depleted at the −1 nucleosome and then rose steadily through the 5′ NDR toward the +1 nucleosome, followed by an immediate downstream dip. This was followed by a steady increase in occupancy toward the 3′ end, with a sharp decrease at the 3′ NDR. Interestingly, the pattern of H1 binding was distinct from that of H3 in all analyzed groups of genes. The peak of H1 around the TSS and the neighboring upstream dip appeared slightly shifted in the 5′ direction in relation to the H3 peak and the 5′ NDR. The resolution of our data is not sufficient to establish whether this could be due to distinct DNA-binding positions of H1 and H3, with H1 binding to linker DNA upstream of H3. In addition, the gene

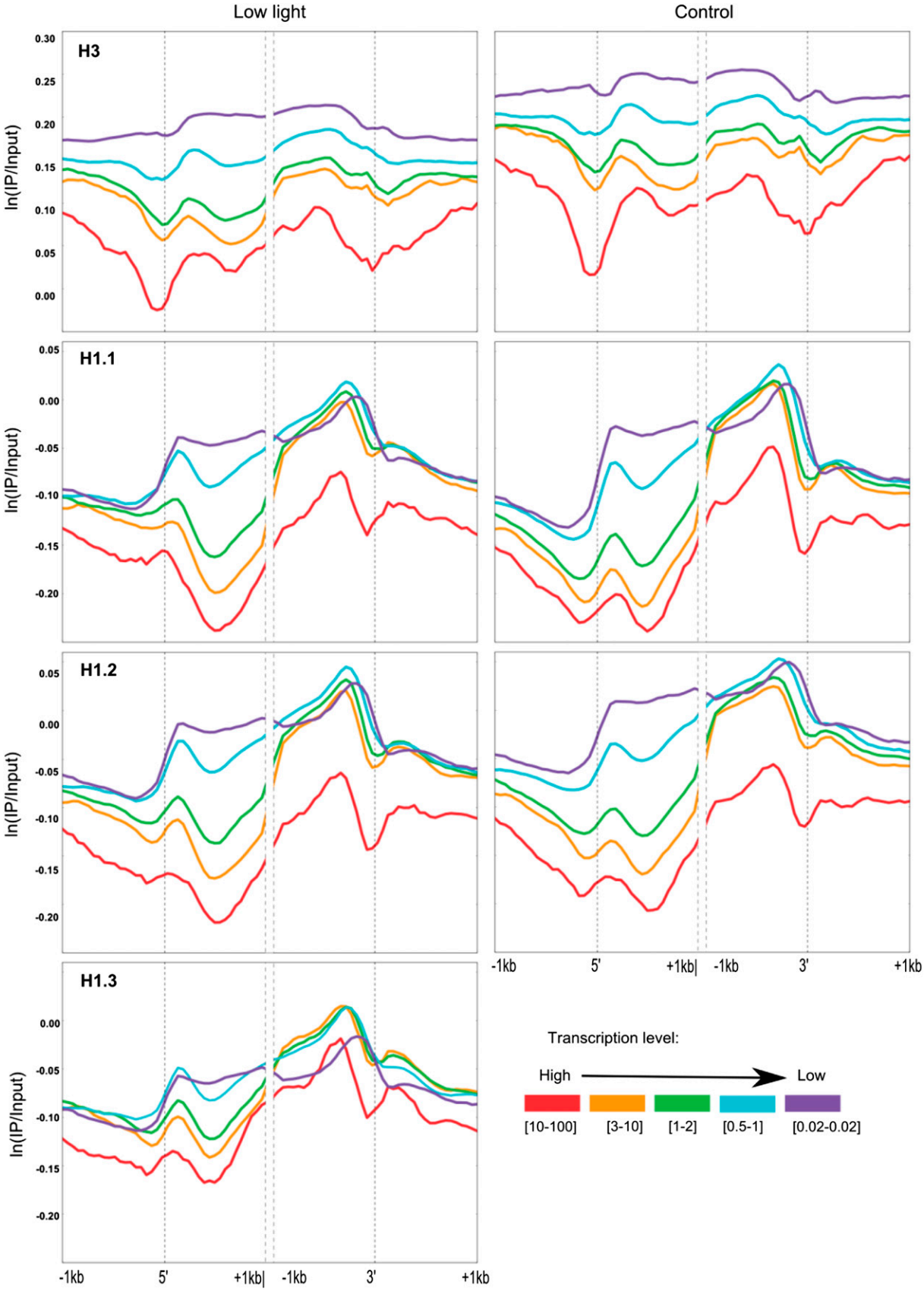

Figure 6. Distribution of H1s and H3 within genes according to their levels of transcription in control conditions and low light. The signal for histone occupancy was plotted for 1 kb around both the 5′ (transcription start site [TSS]) and 3′ ends for five classes of genes divided according to their expression levels. IP, Immunoprecipitate.

bodies (especially in highly expressed histone H3 with trimethylated lysine4 [H3K4me]-marked genes) were not evenly covered by the H1 ChIP signal, suggesting that not all nucleosomes within the gene contain H1 at the same time. Moreover, nucleosomes close to the 5′ ends of active genes were more often depleted in H1 than those at the 3′ ends. The increasing H1 occupancy toward the 3′ end of genes seems to be specific for plants, since no such feature was reported for human or *Drosophila melanogaster* H1s (Braunschweig et al., 2009; Izzo et al., 2013). The question of whether this is related to transcription elongation and/or termination requires further investigation.

Importantly, apart from the inverse relationship between H1.3 binding and the level of gene expression, we detected no qualitative differences among the H1 variants in their patterns of binding along genes in both control and low-light conditions, suggesting that the functions of H1.3 depend largely on its competition with the main H1s for the same binding sites (Fig. 5).

To identify the possible underlying causes of H1.3 chromatin-binding site preferences, we analyzed the distribution of H1s in low light in relation to the known locations of H3K4me3 and H3K9me2 (histone H3 with dimethylated lysine9) methylation marks (Moissiard et al., 2012; Luo et al., 2013). In normal growth conditions, over 16,500 Arabidopsis genes were reported as H3K4me3 tagged and over 3,300 transposable elements (TEs) and genes as H3K9me2 tagged (van Dijk et al., 2010; Zhou et al., 2010). Importantly, in both Arabidopsis and rice (*Oryza sativa*), most of these genes were shown to remain tagged under stress conditions, including drought and decreased light (Guo et al., 2008; van Dijk et al., 2010; Zong et al., 2013). In accordance with their preferred localization in heterochromatin, all three H1 variants were negatively correlated with H3K4me3, an epigenetic mark associated with active chromatin. However, compared with H1.1 and H1.2, H1.3 was clearly less strongly anticorrelated with high levels of H3K4me3 (Fig. 7A), and unlike H1.1 and H1.2, the occupancy of H1.3 at both the 5′ and 3′ ends of genes marked with H3K4me3 was highest on those with the highest level of this modification (Fig. 7B; Supplemental Fig. S17). In contrast, its occupancy on genes marked with H3K9me2 was lowest on those with the highest level of this mark (Fig. 7C; Supplemental Fig. S18). Thus, while it is evident from Figure 7A that, globally, most H1.3 is localized in heterochromatin, as expected for H1 histones, it seems to have an increased potential, compared with the main variants, to bind to sites enriched in epigenetic signatures of active chromatin. Together, our global mapping showed that the overall mode of binding is conserved between the main and stress-inducible H1 variants, indicating the potential for genome-wide competition. While localized mostly in heterochromatin, the members of these two subclasses seem to differ in their preferences for epigenetic signatures of active and inactive chromatin. In contrast to the main variants, the stress-inducible H1.3 shows a greater capability to associate with chromatin enriched in H3K4me3-marked genes.

H1.3 Affects the Level and Targeting of Stress-Dependent DNA Methylation

In both plants (Wierzbicki and Jerzmanowski, 2005; Zemach et al., 2013) and animals (Fan et al., 2005; Yang et al., 2013), H1 has been shown to be involved in establishing and maintaining patterns of DNA methylation. It was recently reported that the main Arabidopsis H1 variants, H1.1 and H1.2, restrict the access of methyltransferases to nucleosomal DNA and that the ATP-dependent nucleosome remodeler DECREASE OF DNA METHYLATION1 (Jeddeloh et al., 1998; Brzeski and Jerzmanowski, 2003) plays a major role in overcoming this restriction and enabling the occurrence and maintenance of DNA methylation, especially within heterochromatin TEs (Zemach et al., 2013). In order to assess the potential contribution of the stress-inducible H1.3 variant to these changes under normal growth conditions, we compared genome-wide DNA methylation patterns in seedlings of wild-type plants and an Arabidopsis line lacking all three H1s. In plants, cytosines are methylated in three different sequence contexts: CG, CHG, and CHH (where H denotes adenine, cytosine, or thymine). The global distribution of DNA methylation on transposons in the triple *h1.1h1.2h1.3* mutant was found to be similar to that reported for a double *h1.1h1.2* mutant (Zemach et al., 2013; Supplemental Fig. S19; Supplemental Tables S5 and S6), consistent with the limited global role of H1.3 in affecting DNA methylation under normal (non-H1.3-inducing) growth conditions. We then examined whether the regime of combined low light/drought used in this study, referred to as stress conditions under which H1.3 is strongly induced, produced alterations in DNA methylation and if any of the observed changes were dependent on H1.3. To this end, we compared the effect of stress on the global level of DNA methylation in the CG, CHG, and CHH contexts in wild-type plants and the *h1.3* mutant by bisulfite sequencing (BS-seq). Overall, stress treatment resulted in increased total DNA methylation, which is consistent with the recent finding that hypermethylation is the prevalent mode of differential methylation in Arabidopsis grown at low water potential (Colaneri and Jones, 2013). Our analysis established the average level of DNA methylation at hundreds of locations. The fluctuations in such averages are naturally quantitatively low but measurable, reproducible between replicates, and statistically significant. We found that the relative increase was moderate in the CG context (2.5%), higher in the CHG context (9.3%), and particularly pronounced in the CHH context (31.8%; Fig. 8A).

As expected, in *h1.3* mutant plants in control conditions, the absence of H1.3 affected the global DNA methylation level only slightly, as revealed by the small

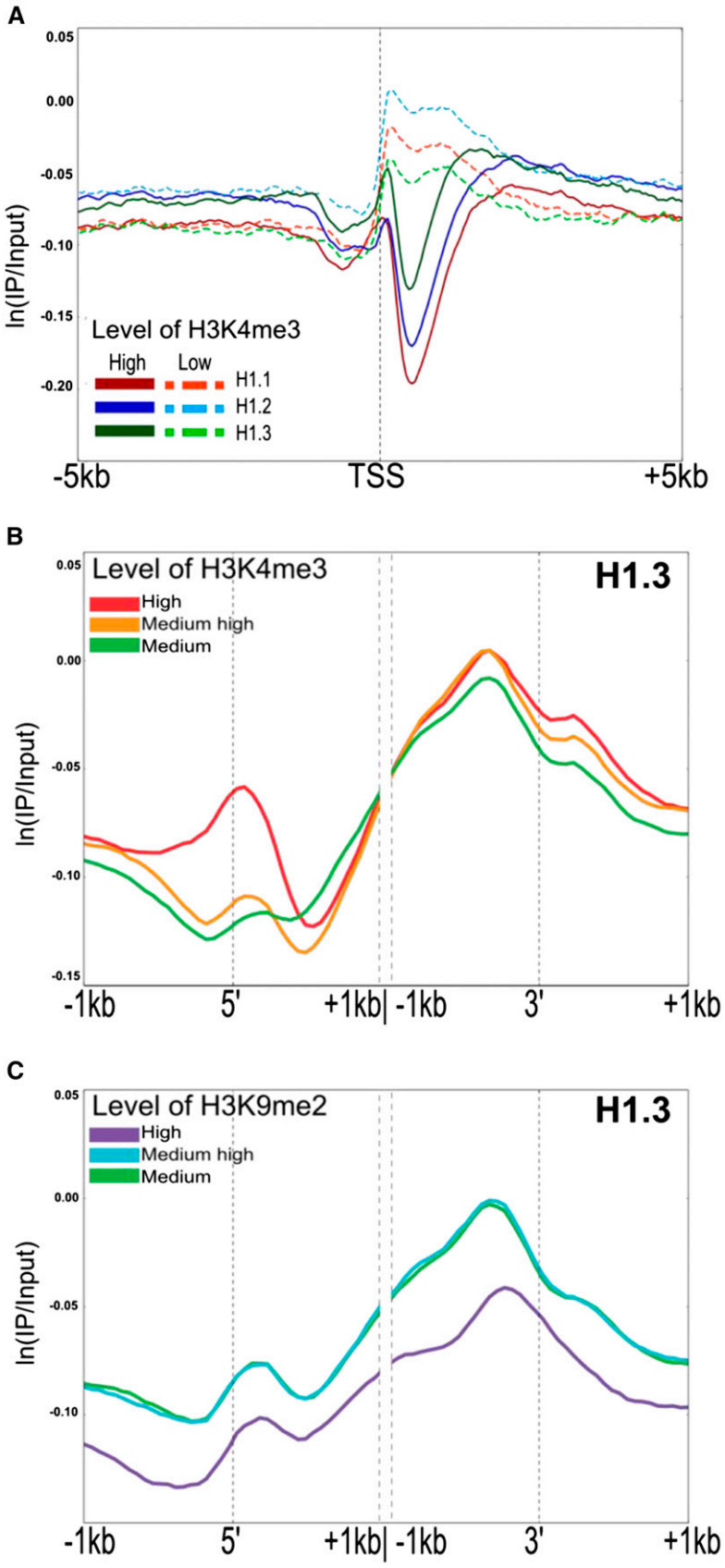

Figure 7. Occupancy of linker histone variants in the Arabidopsis genome. A, H1 occupancies in low light observed for 5 kb around the TSS for a group of 4,495 genes with the highest and 5,999 genes with the lowest levels of H3K4me3. B, H1.3 distribution among genes divided according to the level of H3K4me3. C, H1.3 distribution among genes divided according to the level of H3K9me2. IP, Immunoprecipitate.

overall hypomethylation in the CHG context. However, the lack of H1.3 significantly diminished stress-related DNA methylation, with the most pronounced relative decrease in the CHH context (Fig. 8A; Supplemental Table S7).

From our whole-genome methylome data, we identified genic and nongenic sequences with methylation signatures in all three contexts that increased most significantly in wild-type plants in response to stress. Closer inspection of these stress-responsive loci showed that, in control conditions, their basal methylation level in *h1.3* plants was slightly higher than in the wild type. However, upon stress, these loci did not respond in the *h1.3* mutant as dramatically as in the wild type. This applied to all contexts, suggesting that H1.3 may be required for the occurrence of this increased methylation (Fig. 8B; Supplemental Fig. S20).

We next examined which chromatin regions are differentially methylated upon stress in the wild-type and *h1.3* mutant lines. In Arabidopsis, transposons comprise at least 10% of the genome (i.e. one-fifth of the intergenic DNA; Arabidopsis Genome Initiative, 2000). The analysis of two sets of transposons, one with high (heterochromatic TEs) and the other with low (euchromatic TEs) levels of H3K9me2, showed that, upon exposure to stress, changes in DNA methylation in both wild-type and *h1.3* mutant lines affected the former TEs to a much greater extent than the latter (Supplemental Fig. S21).

In wild-type plants, among 5,030 differentially methylated regions (DMRs) most strongly affected in the CHH context in response to stress, 2,908 were TEs and 371 were genes (sometimes a single DMR contained both a TE and a gene). In the *h1.3* mutant, in the same CHH context, the 3,742 DMRs included 2,217 TEs and 270 genes. For both wild-type and *h1.3* plants, Gene Ontology (GO) analysis of genes present in DMRs did not reveal any specific functional classes, in particular those related to stress responses. However, an examination of the specific types of TEs enriched in DMRs in the CHH context revealed that, in response to stress, there were relatively fewer transposons of the Rolling-Circle/Helitron family in the *h1.3* line compared with the wild type, while the opposite was true for transposons of the Long Terminal Repeat/Gypsy family.

While the proportion of TEs to genes in stress-related DMRs appeared similar in the wild type and *h1.3* mutants (about 8:1), the overlap of methylated sequences between these two lines is only 25%. Thus, the loss of H1.3 significantly affected not only the amount, but also the sequence specificity, of stress-related CHH methylation.

DISCUSSION

Localization and in Vivo Properties of H1 Variants as Revealed Using H1-GFP Fusion Proteins

Rather than studying H1 transcript abundance, we analyzed transgenic Arabidopsis lines expressing fusions of GFP with each of the three H1 variants under the control of their native promoters. This showed that the stress-inducible H1.3 protein occurs in Arabidopsis as two apparently independent pools, which we defined as the constitutive and facultative pools. The former is restricted to guard cells, in which H1.3 occurs under both normal and stress conditions, while the latter includes H1.3, which appears only upon induction and is localized in various tissues and organs. This is in stark contrast to the main variants, H1.1 and H1.2, which are stably expressed throughout the plant. The occurrence of a constitutive guard cell-specific H1.3 pool is consistent with earlier microarray expression data showing that, under normal growth conditions, the *H1.3* transcript is the second most abundant of 64 transcripts preferentially expressed in Arabidopsis guard cells but not in mesenchymal cells (Leonhardt et al., 2004). We found that, as in water stress conditions, ABA is a major positive determinant of the facultative pool of H1.3 induced by low-light stress. Thus, might ABA also be responsible for maintaining the constitutive pool of this protein in guard cells? While this still requires experimental confirmation, we consider such a possibility highly plausible in the light of a recent report that guard cells are capable of autonomous ABA synthesis (Bauer et al., 2013). Moreover, the earlier finding that the level of *H1.3* transcript in guard cells did not change upon ABA treatment (Leonhardt et al., 2004) suggests that it is already at saturation level and that the constitutive H1.3 pool in guard cells may not be significantly affected by stress.

Our FRAP analyses of the in vivo behavior of H1 variants in nuclei revealed that H1.3 binds chromatin with significantly faster dynamics than the more slowly exchanging main variants, particularly the dominant variant H1.2, and in contrast to the main variants, it shows no stable bound pool. To better understand the possible underlying causes of the differences in chromatin binding between the main and stress-inducible linker histone variants, we compared (1) their overall protein organization (Supplemental Fig. S11A) and (2) three-dimensional (3D) molecular models of their conserved globular domains (GH1s; Supplemental Fig. S11, B and C). The CTD of H1.3 is about 50% shorter and has a reduced overall positive charge compared with those of H1.1/2 (Supplemental Fig. S22). Both the N-terminal domain and the CTD of Arabidopsis H1.3 lack the (S/T)PXK motifs that enhance DNA binding and are present in the corresponding domains of H1.1 and H1.2 (Supplemental Fig. S11). The GH1s of the H1.1/2 and H1.3 types differ by a minor alteration of three amino acids that provides the basis for phylogenetic separation of the two protein clades. The amino acids Glu-66, Arg-112, and Ser-116 in H1.1/2-type histones become Phe-28, Asn-75, and Lys-79 in H1.3-type histones. Interestingly, these three amino acids are located close to each other on the surface of GH1 (Supplemental Fig. S11). In addition, Arg-112 in Arabidopsis H1.1/2 corresponds to Arg-74 in the human H10 histone variant, identified as a binding site 1 residue by Brown et al. (2006). The remaining two amino

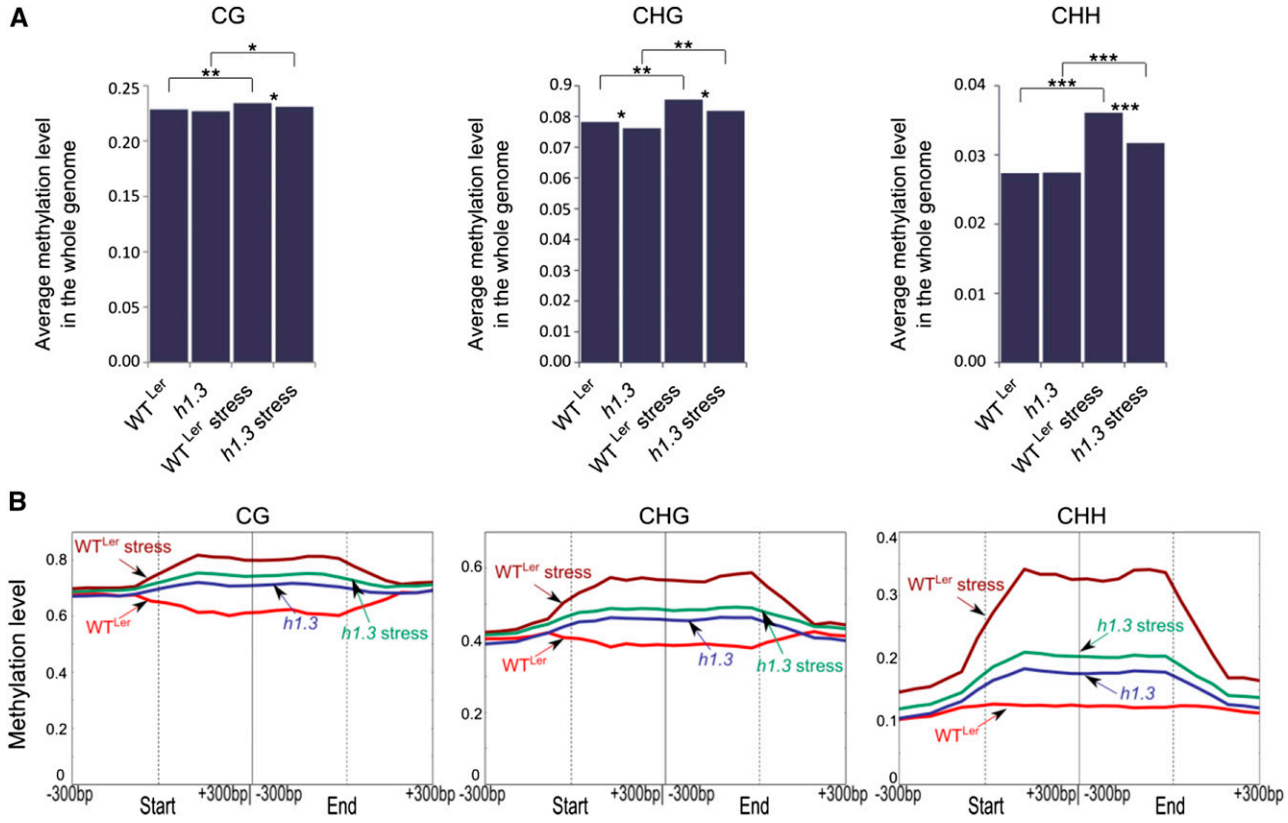

Figure 8. H1.3 is required for de novo DNA methylation in response to low light/drought. A, Averaged DNA methylation levels in the CG, CHG, and CHH contexts in wild-type (WT^{Ler}) and *h1.3* Arabidopsis in control and in low-light/drought conditions (stress). Asterisks indicate levels of significance: ***, $P < 10^{-256}$; **, $P < 10^{-30}$; and *, $P < 10^{-10}$ (Student's *t* test). B, Patterns of DNA methylation (in the CG, CHG, and CHH contexts) in regions that are hypermethylated in response to stress for wild-type and *h1.3* plants in control and in low-light/drought conditions. Averaged methylation (within a sliding 50-bp window) was plotted for 300 bp around both the start and the end of the regions.

acids, Glu-66/Phe-28 and Ser-116/Lys-79, are located between residues corresponding to DNA binding site 1 (His-62, Arg-103, Lys-104, Lys-111, Arg-112, Lys-121, and Lys-123 in H1.1/2; His-24, Arg-66, Lys-67, Lys-74, Lys-84, and Lys-86 in H1.3) and binding site 2 (Arg-79, Lys-127, and Lys-118 in H1.1/2; Lys-41, Lys-90, and Lys-81 in H1.3). We conclude that these amino acid replacements, together with the shortened CTD, could influence the binding of H1.3 and explain its increased mobility.

Another recent study utilizing FRAP showed that H1 chromatin binding is dynamic, with a significant fraction of H1 molecules being partially bound in metastable states that can be readily competed against (Stasevich et al., 2010). Indeed, in addition to its molecular structure and posttranslational modifications, one of the key factors affecting the interaction of H1 with chromatin is competition for specific chromatin-binding sites. The incremental increase in the concentration of competitors, like other H1 variants or High Mobility Group (HMG) proteins, was shown to lead to a new steady state with a shorter H1 chromatin residence time (Catez et al., 2004, 2006). H1.3, which in most tissues increases incrementally upon stress, shows exceptionally high mobility, and lacks any stable bound fraction, is ideally suited to act as a general competitor with the main H1 variants throughout the entire chromatin fiber. Interestingly, under stress conditions, we observed shortening of the residence time of the dominant H1.2 variant in nonguard cell tissues, which approached the value of its typical residence time in guard cells. This raises the question of whether the potential effect of H1.3 as a competitor is spread evenly among all H1 binding sites or shows some degree of specificity. To address this issue, we mapped the distribution of all three H1 variants along Arabidopsis chromosomes. The measurement of genome-wide histone occupancy preferences by ChIP-chip was not expected to yield localized enrichment comparable to that seen for specifically targeted binding proteins such as RNA polymerase. However, we did observe clear and statistically significant differences between the profiles of the H1 variants on large groups of genes and other sequences. As expected for linker histones, both the main and stress-inducible variants were highly enriched in heterochromatin, but they also occurred in

genic regions. Notably, the proportions of relative enrichment between the stress-inducible and main variants changed in favor of the former in genic compared with typical heterochromatin regions. Interestingly, we observed differences in the distribution of intensity profiles along chromosomes between the main and stress-inducible variants that were consistent with patterns of staining with H1 variant-specific antibodies (Ascenzi and Gantt, 1999b) and imply some underlying differences in chromatin localization preferences.

To elucidate the possible reasons for these differences, we analyzed correlations between the distribution of H1 variants and the known distribution profiles of H3K4me3 and H3K9me2 methylation marks, the functionally opposed epigenetic signatures associated with transcriptionally active and repressive chromatin states, respectively. Besides the generally similar tendency of all three H1 variants to accumulate in H3K9me2-rich heterochromatin, H1.3 showed by far the weakest negative correlation with the functionally opposite H3K4me3 epigenetic mark (Fig. 7A). Moreover, and in contrast to H1.1 and H1.2, among genes known to be enriched in H3K4me3, H1.3 showed a marked preference for those with the highest level of this mark. This suggests that, upon induction, H1.3 may compete particularly strongly with the main variants in heterochromatin regions in which the H3K4me3 signatures of past or present transcription have been retained. A more in-depth analysis is required to explain the increased preference of H1.3, in relation to the main variants, for H3K4me3-marked chromatin. This could involve examination of the binding properties of Arabidopsis H1 variants to in vitro reconstituted nucleosomes.

In summary, our data reveal two likely separate and autonomous pools of H1.3 in Arabidopsis: a constitutive guard cell pool and an environmentally regulated facultative pool in other tissues. The superfast binding dynamics and lack of a stable bound fraction of H1.3 shown by FRAP analysis confer significant advantages for a potential competitor targeting H1 binding sites in chromatin. In addition, our mapping of global H1.3 occupancy in chromatin reveals that, while binding mostly within heterochromatin, this linker histone shows a measurable preference, in comparison with the main variants, for chromatin with epigenetic signatures of active transcription. These findings raise the interesting question of whether the role of the inducible pool of H1.3 in nonguard cell tissues is the same or different from the role it plays in guard cells.

The ratio of nonsynonymous substitutions per nonsynonymous site to synonymous substitutions per synonymous site (Ka/Ks) for the main and stress-inducible H1 variants of Arabidopsis is 0.29, which is consistent with strong purifying selection acting on proteins of the two clades and suggests that this diversification plays an adaptive role. Interestingly, we found an early separation of the main and stress-inducible variants, broadly coincidental with an ancient gene or even genome duplication in the common ancestor of extant angiosperms (Jiao et al., 2011). *Amborella trichopoda*, a member of the Amborellales, the earliest angiosperm branch (Magnoliophyta), has both H1.1/2-like and H1.3-like variants, with their characteristic globular domains and differences in the length of their CTDs. However, the GH1s from mosses, ferns, and gymnosperms cannot be precisely classified into main and stress-inducible variants (Supplemental Figs. S12–S14).

Consequences of Depletion of the H1.3 Variant under Normal and Stress Conditions

The availability of *h1.3* null mutant lines enabled the assessment of the role of H1.3 in plants grown in normal and stress conditions. We found that wild-type and *h1.3* plants grown under nonstress conditions were of similar size, but the mutant plants showed a reduced CO_2 assimilation rate and their young leaves had a decreased stomatal density. Comparison of the transcriptomes of wild-type and *h1.3* plants grown under nonstress conditions showed that, among genes with altered transcription in the mutant, there was a significant enrichment of those known to be expressed specifically in guard cells or in guard cells and other tissues, many of which have been linked with guard cell functions. Given the constitutive occurrence of H1.3 in guard cells, this finding suggests that it could be involved in controlling at least some genes specifically expressed in these cells and is probably required for their normal physiological functions. Strikingly, the genes misregulated in the *h1.3* mutant also included major regulators of stomatal biogenesis, known to be expressed in stomatal progenitor cells rather than in mature guard cells. While the direct involvement of H1.3 in the regulation of these genes cannot be excluded, it is also possible that the observed effect is indirect and results from some negative influence on stomatal development in younger leaves, exerted by physiologically impaired guard cells in mature leaves (Lake et al., 2001).

To increase the chances of identifying differences in the responses of wild-type and *h1.3* mutant plants to environmental perturbations, we subjected these plants to combined low-light and water stress, as both treatments cause the induction of H1.3. Surprisingly, we found that a combination of the two stresses led to a synergistic rather than an additive increase in the level of H1.3 induction. Moreover, there were notable differences between wild-type and *h1.3* plants in their responses to combined stress. The typical adaptive developmental response of Arabidopsis to mild water deficiency (i.e. growth retardation resulting mainly from decreased accumulation of biomass after stomatal closure) was visibly hampered in *h1.3* plants, which had a higher leaf number and larger dry and fresh mass compared with wild-type plants. Acceleration of generative development, another adaptation to stress, was also hampered in *h1.3* plants. Overall, the *h1.3* plants reacted as if they were unable to mount a typical

adaptive response to drought stress. With regard to biomass accumulation, the maximum capacity of leaves for exchanging CO_2 and water is mainly determined by short-term regulation of stomatal aperture and long-term regulation of their density through the control of stomatal development (Doheny-Adams et al., 2012). Compared with the wild type, *h1.3* plants showed a decreased ability to respond to combined stress by down-regulating stomatal density, which may indicate their impaired potential for adjusting stomatal development to a changing environment. Again, as indicated above with respect to the decreased stomatal density in *h1.3* plants in nonstress conditions, the role of H1.3 in this regulation may be either direct or indirect and has yet to be determined. In the short term, the regulation of stomatal function might have been directly affected by the aberrant activity of some guard cell-specific genes misregulated in H1.3-depleted plants. However, the impairment of stomatal function and probably stomatal development as well may not be the only causes of the observed lack of adaptive developmental plasticity in response to low-light/drought stress. Our analysis showed that the transcriptional response of *h1.3* mutants to combined stress differed considerably from that of wild-type plants and revealed that, in the absence of H1.3, 70% of over 1,700 affected transcripts were down-regulated. Therefore, it is possible that the growth habit of *h1.3* plants under stress could also be partly due to defects in nonstomatal stress response pathways. Importantly, the normal stress response of *h1.3* mutant plants complemented with the *H1.3* gene confirmed that the lack of H1.3 was the major cause of all aspects of the observed phenotypes.

We found that Arabidopsis plants subjected to combined low-light/drought stress responded by increased DNA methylation, particularly in the CHH context. The recent demonstration of the key role of Arabidopsis H1.1 and H1.2 in preventing the access of DNA methyltransferases to chromatin DNA (Zemach et al., 2013) prompted us to examine the role of H1.3 in stress-related changes in DNA methylation. In control conditions, the triple *h1.1h1.2h1.3* mutant showed changes in the global DNA methylation profile that were very similar to those seen in the double *h1.1h1.2* mutant (Zemach et al., 2013). This indicates that H1.3 plays only a minor role in maintaining the pattern of DNA methylation under normal growth conditions. However, the depletion of H1.3 significantly decreased stress-related DNA hypermethylation and affected its sequence localization. This suggests that the stress-induced H1.3 variant may interfere with the suppression of DNA accessibility to methyltransferases caused by H1.1 and H1.2.

CONCLUSION

The properties of the stress-inducible H1.3 variant described in this report are consistent with a function as a general factor capable of facilitating chromatin accessibility, most likely by directly competing for binding sites with the main H1 variants. The strong dependence of the environmentally controlled facultative pool of H1.3 on ABA and decreased light intensity as well as its relative insensitivity to major photoreceptors suggest a major role for retrograde chloroplast-to-nucleus communication in *H1.3* induction. This is consistent with earlier reports that *H1.3* is one of a small number of genes comprising a core response module responsible for plastid-to-nucleus signaling (Glasser et al., 2014) and the regulation of redox homeostasis (Khandelwal et al., 2008). The existence of an autonomous and constitutive guard cell-specific pool of H1.3, as well as the importance of H1.3 in maintaining leaf stomatal density, suggest that chromatin in guard cells may require permanent modulation by this linker histone variant for proper functioning. Further studies are required to uncover the underlying molecular causes and biological significance of the revealed subtle preference of H1.3 for epigenetic signatures of transcriptionally active chromatin and to elucidate the possible role of H1.3 in stomatal development. The fact that stress-inducible linker histones of the H1.3-type subfamily are conserved in angiosperms, but appear to be absent in evolutionarily older plant lineages, indicates that their biological function may have been important in the evolution of the currently most abundant group of plants on Earth.

MATERIALS AND METHODS

Plant Material

We used Arabidopsis (*Arabidopsis thaliana*) lines in the Col-0 ecotype background unless stated otherwise. Mutants *h1.1* (SALK_N628430; Rea et al., 2012) and *h1.2* (GK-116E080) were obtained from the European Arabidopsis Stock Center. *h1.3* in the L*er* background was obtained from the Cold Spring Harbor Laboratory collection (GT18298). The *h1.1h1.2h1.3* triple mutant was obtained by crossing double mutant *h1.1h1.2* with *h1.3* (which had previously been backcrossed four times to the Col-0 background). Primers used for genotyping *h1* mutants are listed in Supplemental Table S7. Double mutants *phyAphyB* and *cry1cry2* were provided by Stanislaw Karpiński (Banas et al., 2011). *aba1* (L*er*) was provided by Tomasz Sarnowski and Csaba Koncz (Strizhov et al., 1997). Transgenic line H2B-YFP (for yellow fluorescent protein) was provided by Klaus Grasser (Launholt et al., 2006). Transgenic lines encoding linker histone variants H1.1 and H1.2 tagged with enhanced GFP (EGFP), promH1.1::H1.1-EGFP and promH1.2::H1.2-EGFP, were described previously (She et al., 2013). The line expressing H1.3 tagged with EGFP was obtained analogously: a genomic fragment containing the promoter, coding region except for the stop codon, and terminator was amplified by PCR using specific primers listed in Supplemental Table S7. The obtained cassette was cloned into vector pCambia0390 carrying the *nopaline synthase promoter:bialaphos resistance* gene. This construct was then introduced into *Agrobacterium tumefaciens* (GV3101). To obtain the prom.H1.3::H1.3-EGFP and *h1.3*/prom.H1.3::H1.3-EGFP lines, wild-type Arabidopsis plants (Col-0 and L*er*) and *h1.3* (L*er*) were transformed using the floral dip method (Clough and Bent, 1998). Transformed seeds were selected on soil sprayed with Basta solution (50 μg mL^{-1}). At least 12 lines with a confirmed GFP signal were obtained for each construct. After segregation analysis, single insertion and homozygous lines from the T3 or T4 generation were identified and used for further experiments (two lines for H1.3-GFP and three lines each for H1.1-GFP and H1.2-GFP). Expression of EGFP-tagged H1s was confirmed using a fluorescence microscope.

Plant Growth and Treatment Conditions

For all analyses, except for the experiments with combined low-light and drought treatments, plants were grown on plates in medium containing

one-half-strength Murashige and Skoog salts (Sigma-Aldrich) and 1% (w/v) agar, pH 5.8, or in soil under long-day conditions (16 h light/8 h dark) at 22°C with 70% relative humidity (RH) and illumination of 120 μmol m^{-2} s^{-1}. For analysis of the effects of limited light (low-light conditions), the intensity of light during the day was reduced to approximately 20 μmol m^{-2} s^{-1} when seedlings were 21 d old, and the plants were kept in these conditions for 4 d. To investigate morphological and physiological responses to combined low light and drought, plants were sown in 27- to 30-mm-diameter Jiffy expandable peat pots. At the third-leaf stage (16 d after sowing), six peat pots were buried in a single large plastic pot (4.5 dm^3) filled with a strong loamy sand:sand mixture (7:2, v/v). In each large pot, plants of *h1.3*, its sibling wild type, and *h1.3* complemented with prom.H1.3::H1.3-EGFP (*h1.3*/H1.3-GFP) were placed in equal numbers. At this stage, only one plant of equal size was left in each single peat pot. Immediately, or after 2 weeks of growth (25°C, photon flux density of 250 μmol m^{-2} s^{-1} provided by High Pressure Sodium lamps [Agro; Philips], photoperiod of 14/10 h, RH = 40%), the plants were divided for four experimental series (light source, photoperiod, and RH as before): control (400 μmol m^{-2} s^{-1}) or low light (40 μmol m^{-2} s^{-1}) combined with one of two watering regimes: control (60% field water capacity regulated by daily water supplementation to maintain an equal mass) or drought (field water content in soil gradually reduced to 20% field water capacity; water controlled daily, as for the control). The treatments were applied for 17 d, after which growth/physiological analyses were performed.

Measurements of Physiological and Morphological Parameters

Each parameter was measured for at least eight replicate plants for the wild type, *h1.3* mutant, and complemented *h1.3* mutant (*h1.3*/H1.3) grown under control and low-light/drought conditions.

Net Photosynthetic Rate

Net photosynthetic rate was measured using an infrared gas analyzer (Ciras-1; PP Systems) with a whole-plant chamber (200 cm^3). The irradiation system was equipped with halogen lamps. The flow rate of air with a constant CO_2 concentration [400 μmol (CO_2) mol^{-1} (air)] through the assimilation chamber was 600 cm^3 min^{-1}. Measurements were performed at 25°C (leaf temperature) at photon flux density of 500 μmol (quanta) m^{-2} s^{-1} and RH of 50%. The A net photosynthetic carbon assimilation rate value was then calculated (Parkinson et al., 1980).

Water Relations

Water relations in leaves were characterized by determining the RWC and WC. Measurements were performed using all leaves detached from the plants. RWC was determined using the equation $RWC = (FW - DW) \times (TW - DW)^{-1} \times 100\%$ (Klepper and Barrs, 1968), where FW is fresh weight, DW is dry weight, and TW is turgid weight. To measure turgid weight, leaves were placed in darkness for 24 h in vials containing water, at 5°C, to permit complete rehydration. Plant material was dried at 70°C. WC was calculated as $WC = (FW - DW) \times DW^{-1} \times 100\%$.

Analysis of Plant Growth

Analysis of plant growth included recording of the following parameters: leaf number, stem length, leaf area, and fresh and dry weight of leaves and stems. Leaf area was measured using a scanner (ScanMaker 3880; Microtek) and Delta-T Skan 2.03 software (Delta-T Devices).

Leaf Chlorophyll Content

Leaf chlorophyll content was measured with a SPAD-502 chlorophyll meter (Konica Minolta). SPAD readings were taken from all leaves larger than the measurement window (2 × 3 mm).

Chlorophyll a Fluorescence

Chlorophyll fluorescence images of whole plants were taken using an imaging fluorometer (FluorCam; PSI; Nedbal and Whitmarsh, 2004). Chlorophyll fluorescence induction kinetics and quenching parameters were evaluated at 20°C and a normal CO_2 molar ratio, with an experimental protocol comprising 20 min of dark adaptation and the following measurements: (1) fluorescence of dark-adapted leaves when all PSII reaction centers are open; (2) fluorescence of dark-adapted leaves when all PSII reaction centers are closed after a light saturating pulse of about 2,000 μmol m^{-2} s^{-1}; (3) steady-state fluorescence in light-exposed leaves after 420 s of actinic light (300 μmol m^{-2} s^{-1}) combined with saturating light pulses given every 25 s; (4) fluorescence of light-adapted leaves when all PSII reaction centers are closed during the last saturating pulse; and (5) fluorescence of light-adapted leaves when all PSII reaction centers are open, measured with the actinic light source switched off after the far-red light pulse. The photochemical quenching coefficient (Klughammer and Schreiber, 1994) and nonphotochemical quenching (Bilger and Björkman, 1991) were then calculated. The actual or effective quantum yield of photochemical energy conversion in PSII (in the light-adapted state) was then defined (Genty et al., 1989).

Determination of ABA Content

ABA was measured by ELISA as described previously (Dubas et al., 2013). For each treatment, at least three independent ABA measurements were performed on pooled samples collected from three different plants.

Sequence Identification and Multiple Sequence Alignment

Arabidopsis proteins possessing a GH1 domain were identified by exhaustive PSI-BLAST searches of the Arabidopsis proteome using the GH1 domain of Arabidopsis histone H1.1 as the query sequence. For each identified Arabidopsis protein, a PSI-BLAST (Altschul et al., 1997) profile (three iterations, threshold of 0.001) was built for its GH1 domain using the National Center for Biotechnology Information nonredundant sequence database and mapped against The Arabidopsis Information Resource (TAIR) database. Plant sequences possessing the GH1 domain were obtained from the National Center for Biotechnology Information nonredundant database by transitive PSI-BLAST searches (three iterations, threshold of 0.001) using all Arabidopsis GH1 proteins as queries. The sequences were classified into Single Myb Histone, HMG, and H1 groups based on sequence similarity in a graphical clustering tool (CLANS; Frickey and Lupas, 2004). Multiple sequence alignment of the GH1 domain was performed using PCMA (Pei et al., 2003) and Mafft (Katoh and Standley, 2013) followed by some manual adjustments. Sequence conservation in the GH1 domain for H1.1/2-like and H1.3-like variants was visualized from the respective multiple sequence alignments using WebLogo (Crooks et al., 2004).

Model Building

To identify an optimal template for GH1 domain model building, the sequences of all Arabidopsis H1 histone variants were submitted to Meta-Server, which is an assembly of various secondary structure prediction and state-of-the-art fold recognition methods. Collected predictions were screened with 3D-Jury (Ginalski et al., 2003), the consensus method of fold recognition servers, and the structure of *Gallus gallus* GH5 protein (pdb|1hst; Ramakrishnan et al., 1993) was chosen as the template. A sequence-to-structure alignment between H1.1, H1.2, and H1.3 histone variants and the template was built manually using the 3D assessment procedure (Ginalski and Rychlewski, 2003), taking into account the predicted secondary structure, hydrophobic profile of the family, and conservation of important residues. Based on the final sequence-to-structure alignment, 3D models of all three Arabidopsis histone H1 variants were built with the MODELER program (Sali and Blundell, 1993). Finally, side-chain rotamers in the models were optimized using the SCWRL4 package (Krivov et al., 2009).

Domain Architecture and Sequence Analysis

To detect other conserved domains in all identified Arabidopsis GH1 domain proteins, their sequences were analyzed with CDD (Marchler-Bauer et al., 2011) and SMART (Letunic et al., 2006). This analysis also included searches for transmembrane segments (with TMHMM2), signal peptides (SignalP; Nielsen et al., 1997), low compositional complexity (CEG; Wootton, 1994), and coiled-coil regions (Coils2; Lupas et al., 1991) as well as internal repeats (Prospero; Mott, 2000). Regions with no significant sequence similarity to known protein domains were submitted to Meta-BASIC (Ginalski et al., 2004) and then to Meta-Server coupled with 3D-Jury. All identified domains were checked for the conservation of essential elements, including the presence of domain-specific residues.

The percentages of positively (Arg and Lys) and negatively (Asp and Glu) charged residues as well as selected hydrophobic amino acids (Val, Leu, and Ile) in Arabidopsis H1 histone variants were established separately for the GH1 domain and N- and C-terminal unstructured regions. The sequences were also searched for the presence of (S/T)PXK DNA-binding motifs. In addition, the charge profile in the CTD was established by calculating the net charge in a 10-amino acid sliding window.

Tree Building

Phylogenetic trees for selected H1 histone variants from Arabidopsis as well as a broader tree for plant histone H1 proteins were calculated with maximum likelihood (PhyML; Guindon et al., 2010). The multiple sequence alignment of the GH1 domain used for phylogeny reconstruction was additionally trimmed to eliminate poorly aligned and thus uninformative regions (TrimAl; Capella-Gutiérrez et al., 2009). Branch support values were calculated using the approximate likelihood-ratio test method (Anisimova and Gascuel, 2006). Trees were drawn with iTOL (Letunic and Bork, 2011). A coding sequence alignment for Ka/Ks ratio estimation was prepared with ParaAT (Zhang et al., 2012b). The Ka/Ks ratio was calculated in KaKs_Calculator using all of the implemented methods (Zhang et al., 2006), and this ratio was averaged over all the predictions. Plant H1 protein sequences were also clustered in the 3D mode in CLANS (Frickey and Lupas, 2004) with a *P* value threshold of 1e-06.

Gene Expression Analysis (RT-qPCR)

Total RNA was isolated using TRI Reagent (Sigma-Aldrich) followed by Turbo DNase treatment (Ambion). The quantity and quality of RNA were measured with a NanoDrop ND1000 spectrophotometer (NanoDrop Technologies) by gel electrophoresis and/or a Bioanalyzer 2100 device (Agilent Technologies). Reverse transcription was performed using random hexamer primers with the Transcriptor First-Strand cDNA Synthesis Kit (Roche). The obtained complementary DNA (cDNA) was diluted and used as the template in quantitative PCR with LightCycler 480 SYBR Green I Master Mix (Roche). Primers used for the amplification of specific cDNAs for expression analysis are listed in Supplemental Table S7. Reactions were run on a Roche Light Cycler 480.

Microarray Gene Expression Experiments

Material was collected from 24-d-old wild-type and *h1.3* seedlings grown under control and 4-d low-light conditions in the first experiment and from the leaves of 5-week-old wild-type and *h1.3* plants grown under control and combined low-light and drought conditions in the second experiment. Total RNA was extracted using TRI Reagent (Sigma-Aldrich) followed by treatment with Turbo DNase (Ambion) and the RiboMinus Plant Kit (Invitrogen) to reduce the ribosomal RNA fraction. The quantity and quality of the isolated RNA were determined using a NanoDrop ND1000 spectrophotometer, and RNA integrity was assessed with a Bioanalyzer 2100 device. A total of 100 ng of RNA was used for cDNA synthesis with the Ambion WT Expression Kit. A total of 5.5 μg of cDNA, after fragmentation and labeling with the GeneChip WT Terminal Labeling Kit (Affymetrix), was hybridized with an Agronomics array (Rehrauer et al., 2010), using the GeneChip Hybridization Wash and Stain Kit, according to the manufacturer's recommendations (Affymetrix). Three biological replicates were examined for each genotype.

Probe intensities for strand-specific signals were extracted using Affymetrix apt-cel software. The signal was normalized separately for each of the three biological replicates, and the average of the replicates for each probe was used. Probe positions were transformed to the TAIR 10 genome assembly, and the average probe signal for all genes, annotated in the TAIR 10 genome release, was calculated. Differential gene expression was computed by taking the logarithm of the Fch between the relevant conditions. Up- and down-regulated genes were defined as those with absolute z-scores for log-Fch of greater than 2. Submission of the microarray data to the ArrayExpress submissions system is in progress.

Fluorescence and Confocal Microscopy

GFP fluorescence was visualized using the Nikon C1 Laser Scanning Confocal System.

FRAP Analysis

FRAP analysis was performed using a Leica TCS-SP2 confocal laser scanning microscope. Analyses were performed for leaves, roots, root meristems, and hypocotyls derived from 21-d-old seedlings of the following lines grown under control and 4-d low-light conditions: promH1.1::H1.1::GFP, promH1.2::H1.2::GFP, promH1.3::H1.3::GFP, and prom35S::H2B::YFP.

Fluorescence intensity was measured for each studied plant after photobleaching. Measurements were taken at 0.6, 0.8, 1, 1.2, and 5 s, and then at 5-s intervals until 70 s after photobleaching, resulting in 18 measurements per nucleus. Several nuclei were examined in this way for each genotype. The raw data were normalized to the 100% value just before the moment of bleaching. The measurements for each genotype were then averaged, resulting in a single curve per genotype, to which the model was fitted. The GFP fluorescence intensity after photobleaching was modeled using the parametric exponential model (Launholt et al., 2006):

$$(*) \qquad frap(t) = \alpha\left(1 - e^{-t/\tau}\right) + \beta$$

The time to half-recovery of the fluorescence intensity, derived directly from the model equation, is marked below as $t_{1/2}$:

$$\alpha\left(1 - e^{-T_{1/2}/\tau}\right) + \beta = \left\{\lim_{t\to\infty}\left[\alpha\left(1 - e^{-t/\tau}\right) + \beta\right] = \alpha + \beta\right\} = \frac{1}{2}\alpha + \beta$$

$$T_{1/2} = \tau\ln(2)$$

Estimation of Model Parameters

Model parameters were obtained using the Newton-Raphson optimization algorithm that minimized the sum of squared deviations between the fitted curve and the measurements. To ensure the optimal starting point for the algorithm, an initial search of 3D parameter space (α, β, and $t_{1/2}$) was performed. Parameters α and β were tested in the interval (0, 1) at intervals of 0.1, and parameter $t_{1/2}$ was tested in the interval (0, 100) at intervals of 1. The first 1,000 combinations that resulted in the lowest objective function value were used as starting points for the optimization algorithm. The solution that provided the best curve fit to the empirical data indicated the vector of model parameters. For unconstrained estimates, the covariance matrix of model parameters is defined by the following formula:

$$\mathbf{\Sigma} = MSE{\star}(\mathbf{H})^{-1}$$

$$MSE = \mathbf{r}^{\mathrm{T}}\mathbf{r}\Big/(n-p)$$

$$\mathbf{r} = (frap(t) - \hat{frap}(t))$$

where $\mathbf{\Sigma}$ is the (3 × 3) parameter's covariance matrix, $\mathbf{H}$ is a numerical approximation of the Hessian matrix (3 × 3) of the objective function, n is the number of observations (18), p is the number of estimable parameters (3), and $\mathbf{r} = (frap(t) - \hat{frap}(t))$ is a vector of residuals that represents the difference between the observed measurement and the fitted value. The optimization was performed with SAS 9.2 software using the IML procedure (SAS Institute), and call nlpnra was used as the optimization algorithm. The mobile fraction for each of the histone variants was calculated (Launholt et al., 2006). Each parameter is provided with the SE of this estimate (these are not 95% confidence intervals). The SE values of the model parameters and estimates of the mobile fraction were obtained from the covariance matrix $\mathbf{\Sigma}$.

ChIP-Chip Experiments

ChIP experiments were performed as described previously (Nelson et al., 2006) with some modifications. The 24-d-old seedlings of wild-type (Col-0), promH1.1::H1.1::GFP, promH1.2::H1.2::GFP, and promH1.3::H1.3::GFP lines, grown under control and 4-d low-light conditions, were used as the source of chromatin. Anti-H3 (ab1791; Abcam) antibody bound to Dynabeads Protein A (Invitrogen) or GFP-Trap-A (Chromotek) was incubated with isolated chromatin. The extracted DNA was resuspended in 100 μL of water. ChIP enrichment for linker histones and H3 targets was determined by quantitative PCR using LightCycler 480 SYBR Green I Master Mix (Roche). Reactions were performed with 2 μL of immunoprecipitated DNA as template. A standard curve was established for each pair of primers. The amount of ChIP DNA was calculated based on the standard curve, and input DNA was used as a control. For ChIP-chip experiments, the extracted DNA was amplified using the WGA2 Kit (Sigma-Aldrich) according to the manufacturer's protocol. A total of 1.5 μg of DNA was used for fragmentation and labeling with the GeneChip WT Terminal

Labeling Kit (Affymetrix). Labeled DNA was hybridized to the Agronomics microarray (Rehrauer et al., 2010) using the GeneChip Hybridization Wash and Stain Kit according to the manufacturer's recommendations (Affymetrix).

Microarray probe signals were extracted using Affymetrix apt-cel software. Signals for both strands were merged, and the replicates were then transformed to TAIR 10 coordinates, normalized and averaged in the same way as the RNA expression data. The ln(immunoprecipitate/input) was computed for every probe, and the significant regions were then called by finding regions of length greater than 15 probes with enrichment greater than 0.5 (excluding at most three faulty probes). Occupancy profiles were computed as average signals for 100-bp windows, beginning at the 5′ and 3′ ends of the respective features, such as the 5′ and 3′ ends of genes. All expression plots were drawn using the Agronomics python package available from http://bioputer.mimuw.edu.pl/software/agronomics.

BS-seq

For global DNA methylation analysis, DNA was extracted from leaves of 5-week-old wild-type and *h1.3* plants grown under control and low-light/drought conditions. BS-seq was performed in the GeneCore Facility Center, EMBL, using an Illumina HiSeq 2000, with a 100-bp read length.

Reads from BS-seq were mapped to the TAIR 10 genome assembly using Bismark software (Krueger and Andrews, 2011). The positions of methylation sites were extracted with Bismark-extractor and filtered to exclude those without coverage of at least 10 reads. The positions were then divided into groups containing cytosine in three different contexts (CG, CHG, and CHH), and the methylation ratios were computed both for each cytosine separately as well as in 50- and 100-bp windows along all chromosomes. The averaged methylation level in each context (CG, CHG, and CHH) throughout the whole genome was calculated for the 100-bp bins.

Data from high-throughput sequencing experiments are being submitted to the ArrayExpress submissions system data collection under the following accession numbers: E-MTAB-2804 for analysis of the genomic distribution of three linker histone variants in Arabidopsis under normal and low-light conditions by ChIP-chip; E-MTAB-2806 for transcriptomic profiling of the response to combined low-light and drought conditions in wild-type and *h1.3* mutant plants; and E-MTAB-2807 for BS-seq of the wild type and the linker histone mutants under control and combined low-light and drought conditions. They are also available at http://bioputer.mimuw.edu.pl/data/H1.

Supplemental Data

The following supplemental materials are available.

Supplemental Figure S1. Characterization of *H1.3* expression.

Supplemental Figure S2. Expression analysis of Arabidopsis H1 with microarray data (AtGenExpress; Kilian et al., 2007).

Supplemental Figure S3. Schematic representation of the promoter regions of genes encoding Arabidopsis histone H1 somatic variants.

Supplemental Figure S4. Characterization of the *h1.3* mutant line.

Supplemental Figure S5. Stomatal density in leaves of wild-type and *h1.3* mutant plants grown in control and drought/low-light conditions.

Supplemental Figure S6. Growth of *h1.3* mutant plants is not restricted in response to low-light/drought treatment, unlike that of wild-type plants.

Supplemental Figure S7. The *h1.3* mutant complemented with H1.3-GFP responds to combined low-light/drought treatment similarly to wild-type plants.

Supplemental Figure S8. ABA content in wild-type and *h1.3* plants in control and combined low-light/drought conditions.

Supplemental Figure S9. Verification by RT-qPCR of gene expression data obtained in microarray experiments examining the effects of combined low-light/drought treatment.

Supplemental Figure S10. RT-qPCR verification of data obtained in microarray experiments comparing gene expression in normal versus combined low-light/drought (stress) conditions.

Supplemental Figure S11. Arabidopsis linker histones belong to two structurally and functionally diversified families.

Supplemental Figure S12. Phylogenetic tree of 196 plant H1 proteins with HMG sequences used as an outgroup.

Supplemental Figure S13. Phylogenetic tree of 274 plant H1 proteins with *Dictyostelium discoideum* H1 protein as an outgroup.

Supplemental Figure S14. CLANS clustering of 274 plant H1 proteins and a two-dimensional image of the clustering results for an interactive graphical representation of Viridiplantae H1 sequences.

Supplemental Figure S15. Genomic profiles for H1 variants in plants grown in control and 4-d low-light conditions.

Supplemental Figure S16. Distribution of H1 variants along Arabidopsis chromosome 1 in control and low-light conditions.

Supplemental Figure S17. Distribution of the main H1s and H3 within genes with different levels of H3K4me3 of plants grown in control and 4-d low-light conditions.

Supplemental Figure S18. Distribution of the main H1s and H3 within genes with different levels of H3K9me2 of plants grown in control and 4-d low-light conditions.

Supplemental Figure S19. Methylation levels in the triple *h1.1h1.2h1.3* mutant.

Supplemental Figure S20. Methylation changes in response to stress in wild-type and *h1.3* mutant plants.

Supplemental Figure S21. Global methylation changes in the *h1.3* mutant.

Supplemental Figure S22. Moving sum plot of the net charge for the C-terminal region of Arabidopsis histone H1 variants.

Supplemental Table S1. Growth analysis and physiological parameters of wild-type and *h1.3* plants in the early-growth-phase experiment.

Supplemental Table S2. Growth analysis and physiological parameters of wild-type and *h1.3* plants, and the *h1.3* mutant complemented with H1.3-GFP, in the late-growth-phase experiment.

Supplemental Table S3. Statistics for H1 enrichment and depletion at genic features.

Supplemental Table S4. Statistics for changes in methylation of euchromatic and heterochromatic TEs.

Supplemental Table S5. Statistics for changes in methylation of euchromatic and heterochromatic genes.

Supplemental Table S6. Statistics for differences in the average global methylation level between genotypes and conditions in three different DNA methylation contexts.

Supplemental Table S7. Sequences of oligonucleotide primers used in this study.

Supplemental Data Set S1. Genes with expression changed in *h1.3* mutant plants in control conditions, comparison with wild-type plants in control conditions, and GO analysis with the agriGO tool (Du et al., 2010).

Supplemental Data Set S2. Genes with expression changed in wild-type plants in low-light/drought conditions, comparison with wild-type plants in control conditions, and GO analysis with the agriGO tool (Du et al., 2010).

Supplemental Data Set S3. Genes with expression changed in *h1.3* mutant plants in low-light/drought conditions, comparison with *h1.3* mutant plants in control conditions, and GO analysis with the agriGO tool (Du et al., 2010).

Supplemental Data Set S4. Genes with expression changed in *h1.3* mutant plants in low-light/drought conditions, comparison with wild-type plants in low-light/drought conditions, and GO analysis with the agriGO tool (Du et al., 2010).

Supplemental Video S1. The dynamics of H1.1-GFP in guard cells during a FRAP experiment.

Supplemental Video S2. The dynamics of H1.2-GFP in guard cells during a FRAP experiment.

Supplemental Video S3. The dynamics of H1.3-GFP in guard cells during a FRAP experiment.

ACKNOWLEDGMENTS

We thank Gideon Grafi, Célia Baroux, and John Gittins for critically reading the article; Klaus D. Grasser for the H2B-YFP transgenic line; Stanisław Karpiński for providing *phyAphyB* and *cry1cry2* mutants; Tomasz Sarnowski and Csaba Koncz for providing the *aba1* mutant; Vladimir Benes and Dinko Pavlinic for support provided in generating DNA methylome sequence data; and Antoni Palusiński for photography expertise.

Received March 31, 2015; accepted September 7, 2015; published September 8, 2015.

LITERATURE CITED

Altschul SF, Madden TL, Schäffer AA, Zhang J, Zhang Z, Miller W, Lipman DJ (1997) Gapped BLAST and PSI-BLAST: a new generation of protein database search programs. Nucleic Acids Res **25:** 3389–3402

Anisimova M, Gascuel O (2006) Approximate likelihood-ratio test for branches: a fast, accurate, and powerful alternative. Syst Biol **55:** 539–552

Arabidopsis Genome Initiative (2000) Analysis of the genome sequence of the flowering plant Arabidopsis thaliana. Nature **408:** 796–815

Ascenzi R, Gantt JS (1997) A drought-stress-inducible histone gene in Arabidopsis thaliana is a member of a distinct class of plant linker histone variants. Plant Mol Biol **34:** 629–641

Ascenzi R, Gantt JS (1999a) Molecular genetic analysis of the drought-inducible linker histone variant in Arabidopsis thaliana. Plant Mol Biol **41:** 159–169

Ascenzi R, Gantt JS (1999b) Subnuclear distribution of the entire complement of linker histone variants in Arabidopsis thaliana. Chromosoma **108:** 345–355

Banas AK, Łabuz J, Sztatelman O, Gabrys H, Fiedor L (2011) Expression of enzymes involved in chlorophyll catabolism in Arabidopsis is light controlled. Plant Physiol **157:** 1497–1504

Bauer H, Ache P, Lautner S, Fromm J, Hartung W, Al-Rasheid KA, Sonnewald S, Sonnewald U, Kneitz S, Lachmann N, et al (2013) The stomatal response to reduced relative humidity requires guard cell-autonomous ABA synthesis. Curr Biol **23:** 53–57

Berendzen SM, Carey JD, Smith EB (2006) Diltiazem-associated photodistributed hyperpigmentation in an elderly Hispanic female. Int J Dermatol **45:** 1450–1452

Bilger W, Björkman O (1991) Temperature dependence of violaxanthin deepoxidation and non-photochemical fluorescence quenching in intact leaves of Gossypium hirsutum L. and Malva parviflora L. Planta **184:** 226–234

Braunschweig U, Hogan GJ, Pagie L, van Steensel B (2009) Histone H1 binding is inhibited by histone variant H3.3. EMBO J **28:** 3635–3645

Brown DT, Izard T, Misteli T (2006) Mapping the interaction surface of linker histone H1(0) with the nucleosome of native chromatin in vivo. Nat Struct Mol Biol **13:** 250–255

Brzeski J, Jerzmanowski A (2003) Deficient in DNA methylation 1 (DDM1) defines a novel family of chromatin-remodeling factors. J Biol Chem **278:** 823–828

Cao K, Lailler N, Zhang Y, Kumar A, Uppal K, Liu Z, Lee EK, Wu H, Medrzycki M, Pan C, et al (2013) High-resolution mapping of H1 linker histone variants in embryonic stem cells. PLoS Genet **9:** e1003417

Capella-Gutiérrez S, Silla-Martínez JM, Gabaldón T (2009) trimAl: a tool for automated alignment trimming in large-scale phylogenetic analyses. Bioinformatics **25:** 1972–1973

Catez F, Ueda T, Bustin M (2006) Determinants of histone H1 mobility and chromatin binding in living cells. Nat Struct Mol Biol **13:** 305–310

Catez F, Yang H, Tracey KJ, Reeves R, Misteli T, Bustin M (2004) Network of dynamic interactions between histone H1 and high-mobility-group proteins in chromatin. Mol Cell Biol **24:** 4321–4328

Chaves MM, Flexas J, Pinheiro C (2009) Photosynthesis under drought and salt stress: regulation mechanisms from whole plant to cell. Ann Bot (Lond) **103:** 551–560

Christophorou MA, Castelo-Branco G, Halley-Stott RP, Oliveira CS, Loos R, Radzisheuskaya A, Mowen KA, Bertone P, Silva JC, Zernicka-Goetz M, et al (2014) Citrullination regulates pluripotency and histone H1 binding to chromatin. Nature **507:** 104–108

Clough SJ, Bent AF (1998) Floral dip: a simplified method for Agrobacterium-mediated transformation of Arabidopsis thaliana. Plant J **16:** 735–743

Cohen A, Bray EA (1990) Characterization of three mRNAs that accumulate in wilted tomato leaves in response to elevated levels of endogenous abscisic acid. Planta **182:** 27–33

Cohen A, Plant AL, Moses MS, Bray EA (1991) Organ-specific and environmentally regulated expression of two abscisic acid-induced genes of tomato: nucleotide sequence and analysis of the corresponding cDNAs. Plant Physiol **97:** 1367–1374

Colaneri AC, Jones AM (2013) Genome-wide quantitative identification of DNA differentially methylated sites in Arabidopsis seedlings growing at different water potential. PLoS One **8:** e59878

Crooks GE, Hon G, Chandonia JM, Brenner SE (2004) WebLogo: a sequence logo generator. Genome Res **14:** 1188–1190

Doheny-Adams T, Hunt L, Franks PJ, Beerling DJ, Gray JE (2012) Genetic manipulation of stomatal density influences stomatal size, plant growth and tolerance to restricted water supply across a growth carbon dioxide gradient. Philos Trans R Soc Lond B Biol Sci **367:** 547–555

Du Z, Zhou X, Ling Y, Zhang Z, Su Z (2010) agriGO: a GO analysis toolkit for the agricultural community. Nucleic Acids Res **38:** W64–W70

Dubas E, Janowiak F, Krzewska M, Hura T, Żur I (2013) Endogenous ABA concentration and cytoplasmic membrane fluidity in microspores of oilseed rape (Brassica napus L.) genotypes differing in responsiveness to androgenesis induction. Plant Cell Rep **32:** 1465–1475

Fan Y, Nikitina T, Zhao J, Fleury TJ, Bhattacharyya R, Bouhassira EE, Stein A, Woodcock CL, Skoultchi AI (2005) Histone H1 depletion in mammals alters global chromatin structure but causes specific changes in gene regulation. Cell **123:** 1199–1212

Fey V, Wagner R, Bräutigam K, Pfannschmidt T (2005) Photosynthetic redox control of nuclear gene expression. J Exp Bot **56:** 1491–1498

Frickey T, Lupas A (2004) CLANS: a Java application for visualizing protein families based on pairwise similarity. Bioinformatics **20:** 3702–3704

Fujita Y, Fujita M, Shinozaki K, Yamaguchi-Shinozaki K (2011) ABA-mediated transcriptional regulation in response to osmotic stress in plants. J Plant Res **124:** 509–525

Genty B, Briantais JM, Baker NR (1989) The relationship between the quantum yield of photosynthetic electron transport and quenching of chlorophyll fluorescence. Biochim Biophys Acta **990:** 87–92

Ginalski K, Elofsson A, Fischer D, Rychlewski L (2003) 3D-Jury: a simple approach to improve protein structure predictions. Bioinformatics **19:** 1015–1018

Ginalski K, Rychlewski L (2003) Protein structure prediction of CASP5 comparative modeling and fold recognition targets using consensus alignment approach and 3D assessment. Proteins (Suppl 6) **53:** 410–417

Ginalski K, von Grotthuss M, Grishin NV, Rychlewski L (2004) Detecting distant homology with Meta-BASIC. Nucleic Acids Res **32:** W576–W581

Glasser C, Haberer G, Finkemeier I, Pfannschmidt T, Kleine T, Leister D, Dietz KJ, Häusler RE, Grimm B, Mayer KF (2014) Meta-analysis of retrograde signaling in Arabidopsis thaliana reveals a core module of genes embedded in complex cellular signaling networks. Mol Plant **7:** 1167–1190

Gómez-Porras JL, Riaño-Pachón DM, Dreyer I, Mayer JE, Mueller-Roeber B (2007) Genome-wide analysis of ABA-responsive elements ABRE and CE3 reveals divergent patterns in Arabidopsis and rice. BMC Genomics **8:** 260

Guindon S, Dufayard JF, Lefort V, Anisimova M, Hordijk W, Gascuel O (2010) New algorithms and methods to estimate maximum-likelihood phylogenies: assessing the performance of PhyML 3.0. Syst Biol **59:** 307–321

Guo L, Zhou J, Elling AA, Charron JB, Deng XW (2008) Histone modifications and expression of light-regulated genes in Arabidopsis are cooperatively influenced by changing light conditions. Plant Physiol **147:** 2070–2083

Harshman SW, Young NL, Parthun MR, Freitas MA (2013) H1 histones: current perspectives and challenges. Nucleic Acids Res **41:** 9593–9609

Izzo A, Kamieniarz-Gdula K, Ramírez F, Noureen N, Kind J, Manke T, van Steensel B, Schneider R (2013) The genomic landscape of the somatic linker histone subtypes H1.1 to H1.5 in human cells. Cell Reports **3:** 2142–2154

Jeddeloh JA, Bender J, Richards EJ (1998) The DNA methylation locus DDM1 is required for maintenance of gene silencing in Arabidopsis. Genes Dev **12:** 1714–1725

Jerzmanowski A, Przewłoka M, Grasser KD (2000) Linker histones and HMG1 proteins of higher plants. Plant Biol **2:** 586–597

Jiang C, Pugh BF (2009) Nucleosome positioning and gene regulation: advances through genomics. Nat Rev Genet **10:** 161–172

Jiao Y, Wickett NJ, Ayyampalayam S, Chanderbali AS, Landherr L, Ralph PE, Tomsho LP, Hu Y, Liang H, Soltis PS, et al (2011) Ancestral polyploidy in seed plants and angiosperms. Nature **473:** 97–100

Jullien J, Astrand C, Halley-Stott RP, Garrett N, Gurdon JB (2010) Characterization of somatic cell nuclear reprogramming by oocytes in which a linker histone is required for pluripotency gene reactivation. Proc Natl Acad Sci USA **107:** 5483–5488

Katoh K, Standley DM (2013) MAFFT multiple sequence alignment software version 7: improvements in performance and usability. Mol Biol Evol **30:** 772–780

Khandelwal A, Elvitigala T, Ghosh B, Quatrano RS (2008) Arabidopsis transcriptome reveals control circuits regulating redox homeostasis and the role of an AP2 transcription factor. Plant Physiol **148:** 2050–2058

Kilian J, Whitehead D, Horak J, Wanke D, Weinl S, Batistic O, D'Angelo C, Bornberg-Bauer E, Kudla J, Harter K (2007) The AtGenExpress global stress expression data set: protocols, evaluation and model data analysis of UV-B light, drought and cold stress responses. Plant J **50:** 347–363

Kinoshita T, Seki M (2014) Epigenetic memory for stress response and adaptation in plants. Plant Cell Physiol **55:** 1859–1863

Klepper B, Barrs HD (1968) Effects of salt secretion on psychrometric determinations of water potential of cotton leaves. Plant Physiol **43:** 1138–1140

Klughammer C, Schreiber U (1994) An improved method, using saturating light pulses, for the determination of photosystem I quantum yield via $P700^+$-absorbance changes at 830 nm. Planta **192:** 261–268

Krivov GG, Shapovalov MV, Dunbrack RL Jr (2009) Improved prediction of protein side-chain conformations with SCWRL4. Proteins **77:** 778–795

Krueger F, Andrews SR (2011) Bismark: a flexible aligner and methylation caller for Bisulfite-Seq applications. Bioinformatics **27:** 1571–1572

Kumari A, Jewaria PK, Bergmann DC, Kakimoto T (2014) Arabidopsis reduces growth under osmotic stress by decreasing SPEECHLESS protein. Plant Cell Physiol **55:** 2037–2046

Lake JA, Quick WP, Beerling DJ, Woodward FI (2001) Plant development: signals from mature to new leaves. Nature **411:** 154

Lau OS, Bergmann DC (2012) Stomatal development: a plant's perspective on cell polarity, cell fate transitions and intercellular communication. Development **139:** 3683–3692

Launholt D, Merkle T, Houben A, Schulz A, Grasser KD (2006) *Arabidopsis* chromatin-associated HMGA and HMGB use different nuclear targeting signals and display highly dynamic localization within the nucleus. Plant Cell **18:** 2904–2918

Leonhardt N, Kwak JM, Robert N, Waner D, Leonhardt G, Schroeder JI (2004) Microarray expression analyses of *Arabidopsis* guard cells and isolation of a recessive abscisic acid hypersensitive protein phosphatase 2C mutant. Plant Cell **16:** 596–615

Lepistö A, Toivola J, Nikkanen L, Rintamäki E (2012) Retrograde signaling from functionally heterogeneous plastids. Front Plant Sci **3:** 286

Letunic I, Bork P (2011) Interactive Tree Of Life v2: online annotation and display of phylogenetic trees made easy. Nucleic Acids Res **39:** W475–W478

Letunic I, Copley RR, Pils B, Pinkert S, Schultz J, Bork P (2006) SMART 5: domains in the context of genomes and networks. Nucleic Acids Res **34:** D257–D260

Lippman Z, Gendrel AV, Black M, Vaughn MW, Dedhia N, McCombie WR, Lavine K, Mittal V, May B, Kasschau KD, et al (2004) Role of transposable elements in heterochromatin and epigenetic control. Nature **430:** 471–476

Luo C, Sidote DJ, Zhang Y, Kerstetter RA, Michael TP, Lam E (2013) Integrative analysis of chromatin states in Arabidopsis identified potential regulatory mechanisms for natural antisense transcript production. Plant J **73:** 77–90

Lupas A, Van Dyke M, Stock J (1991) Predicting coiled coils from protein sequences. Science **252:** 1162–1164

MacAlister CA, Ohashi-Ito K, Bergmann DC (2007) Transcription factor control of asymmetric cell divisions that establish the stomatal lineage. Nature **445:** 537–540

Marchler-Bauer A, Lu S, Anderson JB, Chitsaz F, Derbyshire MK, DeWeese-Scott C, Fong JH, Geer LY, Geer RC, Gonzales NR, et al (2011) CDD: a Conserved Domain Database for the functional annotation of proteins. Nucleic Acids Res **39:** D225–D229

McBryant SJ, Lu X, Hansen JC (2010) Multifunctionality of the linker histones: an emerging role for protein-protein interactions. Cell Res **20:** 519–528

Moissiard G, Cokus SJ, Cary J, Feng S, Billi AC, Stroud H, Husmann D, Zhan Y, Lajoie BR, McCord RP, et al (2012) MORC family ATPases required for heterochromatin condensation and gene silencing. Science **336:** 1448–1451

Mott R (2000) Accurate formula for P-values of gapped local sequence and profile alignments. J Mol Biol **300:** 649–659

Nedbal L, Whitmarsh J (2004) Chlorophyll fluorescence imaging of leaves and fruits. *In* G Papageorgiou, Govindjee, eds, Chlorophyll Fluorescence: A Signature of Photosynthesis. Springer, Dordrecht, The Netherlands, pp 389–407

Nelson JD, Denisenko O, Sova P, Bomsztyk K (2006) Fast chromatin immunoprecipitation assay. Nucleic Acids Res **34:** e2

Nielsen H, Engelbrecht J, Brunak S, von Heijne G (1997) Identification of prokaryotic and eukaryotic signal peptides and prediction of their cleavage sites. Protein Eng **10:** 1–6

Parkinson KJ, Day W, Leach JE (1980) A portable system for measuring the photosynthesis and transpiration of graminaceous leaves. J Exp Bot **31:** 1441–1453

Pei J, Sadreyev R, Grishin NV (2003) PCMA: fast and accurate multiple sequence alignment based on profile consistency. Bioinformatics **19:** 427–428

Pérez-Montero S, Carbonell A, Morán T, Vaquero A, Azorín F (2013) The embryonic linker histone H1 variant of Drosophila, dBigH1, regulates zygotic genome activation. Dev Cell **26:** 578–590

Pfalz J, Liebers M, Hirth M, Grübler B, Holtzegel U, Schröter Y, Dietzel L, Pfannschmidt T (2012) Environmental control of plant nuclear gene expression by chloroplast redox signals. Front Plant Sci **3:** 257

Phair RD, Scaffidi P, Elbi C, Vecerová J, Dey A, Ozato K, Brown DT, Hager G, Bustin M, Misteli T (2004) Global nature of dynamic protein-chromatin interactions in vivo: three-dimensional genome scanning and dynamic interaction networks of chromatin proteins. Mol Cell Biol **24:** 6393–6402

Plant AL, Cohen A, Moses MS, Bray EA (1991) Nucleotide sequence and spatial expression pattern of a drought- and abscisic acid-induced gene of tomato. Plant Physiol **97:** 900–906

Przewloka MR, Wierzbicki AT, Slusarczyk J, Kuraś M, Grasser KD, Stemmer C, Jerzmanowski A (2002) The "drought-inducible" histone H1s of tobacco play no role in male sterility linked to alterations in H1 variants. Planta **215:** 371–379

Raghuram N, Carrero G, Th'ng J, Hendzel MJ (2009) Molecular dynamics of histone H1. Biochem Cell Biol **87:** 189–206

Ramakrishnan V, Finch JT, Graziano V, Lee PL, Sweet RM (1993) Crystal structure of globular domain of histone H5 and its implications for nucleosome binding. Nature **362:** 219–223

Rea M, Zheng W, Chen M, Braud C, Bhangu D, Rognan TN, Xiao W (2012) Histone H1 affects gene imprinting and DNA methylation in Arabidopsis. Plant J **71:** 776–786

Rehrauer H, Aquino C, Gruissem W, Henz SR, Hilson P, Laubinger S, Naouar N, Patrignani A, Rombauts S, Shu H, et al (2010) AGRONOMICS1: a new resource for Arabidopsis transcriptome profiling. Plant Physiol **152:** 487–499

Rosa S, Ntoukakis V, Ohmido N, Pendle A, Abranches R, Shaw P (2014) Cell differentiation and development in *Arabidopsis* are associated with changes in histone dynamics at the single-cell level. Plant Cell **26:** 4821–4833

Sali A, Blundell TL (1993) Comparative protein modelling by satisfaction of spatial restraints. J Mol Biol **234:** 779–815

Schmid M, Davison TS, Henz SR, Pape UJ, Demar M, Vingron M, Schölkopf B, Weigel D, Lohmann JU (2005) A gene expression map of Arabidopsis thaliana development. Nat Genet **37:** 501–506

Scippa GS, Di Michele M, Onelli E, Patrignani G, Chiatante D, Bray EA (2004) The histone-like protein H1-S and the response of tomato leaves to water deficit. J Exp Bot **55:** 99–109

Scippa GS, Griffiths A, Chiatante D, Bray EA (2000) The H1 histone variant of tomato, H1-S, is targeted to the nucleus and accumulates in chromatin in response to water-deficit stress. Planta **211:** 173–181

Shahhoseini M, Favaedi R, Baharvand H, Sharma V, Stunnenberg HG (2010) Evidence for a dynamic role of the linker histone variant H1x during retinoic acid-induced differentiation of NT2 cells. FEBS Lett **584:** 4661–4664

She W, Grimanelli D, Rutowicz K, Whitehead MW, Puzio M, Kotlinski M, Jerzmanowski A, Baroux C (2013) Chromatin reprogramming during the somatic-to-reproductive cell fate transition in plants. Development **140:** 4008–4019

Smith KT, Workman JL (2012) Chromatin proteins: key responders to stress. PLoS Biol **10:** e1001371

Stasevich TJ, Mueller F, Brown DT, McNally JG (2010) Dissecting the binding mechanism of the linker histone in live cells: an integrated FRAP analysis. EMBO J **29:** 1225–1234

Strizhov N, Abrahám E, Okrész L, Blickling S, Zilberstein A, Schell J, Koncz C, Szabados L (1997) Differential expression of two P5CS genes controlling proline accumulation during salt-stress requires ABA and is regulated by ABA1, ABI1 and AXR2 in Arabidopsis. Plant J **12:** 557–569

Talbert PB, Ahmad K, Almouzni G, Ausió J, Berger F, Bhalla PL, Bonner WM, Cande WZ, Chadwick BP, Chan SW, et al (2012) A unified phylogeny-based nomenclature for histone variants. Epigenetics Chromatin **5:** 7

van Dijk K, Ding Y, Malkaram S, Riethoven JJ, Liu R, Yang J, Laczko P, Chen H, Xia Y, Ladunga I, et al (2010) Dynamic changes in genome-wide histone H3 lysine 4 methylation patterns in response to dehydration stress in Arabidopsis thaliana. BMC Plant Biol **10:** 238

van Zanten M, Tessadori F, McLoughlin F, Smith R, Millenaar FF, van Driel R, Voesenek LA, Peeters AJ, Fransz P (2010) Photoreceptors CRYTOCHROME2 and phytochrome B control chromatin compaction in Arabidopsis. Plant Physiol **154:** 1686–1696

Wei T, O'Connell MA (1996) Structure and characterization of a putative drought-inducible H1 histone gene. Plant Mol Biol **30:** 255–268

Wierzbicki AT, Jerzmanowski A (2005) Suppression of histone H1 genes in Arabidopsis results in heritable developmental defects and stochastic changes in DNA methylation. Genetics **169:** 997–1008

Wootton JC (1994) Non-globular domains in protein sequences: automated segmentation using complexity measures. Comput Chem **18:** 269–285

Yang SM, Kim BJ, Norwood Toro L, Skoultchi AI (2013) H1 linker histone promotes epigenetic silencing by regulating both DNA methylation and histone H3 methylation. Proc Natl Acad Sci USA **110:** 1708–1713

Zemach A, Kim MY, Hsieh PH, Coleman-Derr D, Eshed-Williams L, Thao K, Harmer SL, Zilberman D (2013) The Arabidopsis nucleosome remodeler DDM1 allows DNA methyltransferases to access H1-containing heterochromatin. Cell **153:** 193–205

Zhang Y, Cooke M, Panjwani S, Cao K, Krauth B, Ho PY, Medrzycki M, Berhe DT, Pan C, McDevitt TC, et al (2012a) Histone H1 depletion impairs embryonic stem cell differentiation. PLoS Genet **8:** e1002691

Zhang Z, Li J, Zhao XQ, Wang J, Wong GK, Yu J (2006) KaKs_Calculator: calculating Ka and Ks through model selection and model averaging. Genomics Proteomics Bioinformatics **4:** 259–263

Zhang Z, Xiao J, Wu J, Zhang H, Liu G, Wang X, Dai L (2012b) ParaAT: a parallel tool for constructing multiple protein-coding DNA alignments. Biochem Biophys Res Commun **419:** 779–781

Zhou J, Wang X, He K, Charron JB, Elling AA, Deng XW (2010) Genome-wide profiling of histone H3 lysine 9 acetylation and dimethylation in Arabidopsis reveals correlation between multiple histone marks and gene expression. Plant Mol Biol **72:** 585–595

Zimmermann P, Hirsch-Hoffmann M, Hennig L, Gruissem W (2004) GENEVESTIGATOR: Arabidopsis microarray database and analysis toolbox. Plant Physiol **136:** 2621–2632

Zong W, Zhong X, You J, Xiong L (2013) Genome-wide profiling of histone H3K4-tri-methylation and gene expression in rice under drought stress. Plant Mol Biol **81:** 175–188